PHYSICS OF THE EXTENDED NEURON*

P C BRESSLOFF† and S COOMBES‡

Nonlinear and Complex Systems Group,

Department of Mathematical Sciences,

Loughborough University,
Loughborough, Leicestershire, LE12 8DB, UK

Received 27 March 1997

We review recent work concerning the effects of dendritic structure on single neuron response and the dynamics of neural populations. We highlight a number of concepts and techniques from physics useful in studying the behaviour of the spatially extended neuron. First we show how the single neuron Green's function, which incorporates details concerning the geometry of the dendritic tree, can be determined using the theory of random walks. We then exploit the formal analogy between a neuron with dendritic structure and the tight–binding model of excitations on a disordered lattice to analyse various Dyson–like equations arising from the modelling of synaptic inputs and random synaptic background activity. Finally, we formulate the dynamics of interacting populations of spatially extended neurons in terms of a set of Volterra integro–differential equations whose kernels are the single neuron Green's functions. Linear stability analysis and bifurcation theory are then used to investigate two particular aspects of population dynamics (i) pattern formation in a strongly coupled network of analog neurons and (ii) phase–synchronization in a weakly coupled network of integrate–and–fire neurons.

1. Introduction

The identification of the main levels of organization in synaptic neural circuits may provide the framework for understanding the dynamics of the brain. Some of these levels have already been identified[1]. Above the level of molecules and ions, the synapse and local patterns of synaptic connection and interaction define a microcircuit. These are grouped to form dendritic subunits within the dendritic tree of single neurons. A single neuron consists of a cell body (soma) and the branched processes (dendrites) emanating from it, both of which have synapses, together with an axon that carries signals to other neurons (figure 1). Interactions between neurons constitute local circuits. Above this level are the columns, laminae and topographic maps involving multiple regions in the brain. They can often be associated with the generation of a specific behaviour in an organism. Interestingly it has been shown that sensory stimulation can lead to neurons developing an extensive dendritic tree. In some neurons over 99% of their surface area is accounted for in the dendritic tree. The tree is the largest volumetric component of neural tissue in the brain, and with up to 200,000 synapses consumes 60% of the brains energy[2].

*Preprint version of review in Int. J. Mod. Phys. B, vol. 11 (1997) 2343-2392
†P.C.Bressloff@Lboro.ac.uk
‡S.Coombes@Lboro.ac.uk
PACS Nos: 84.10+e

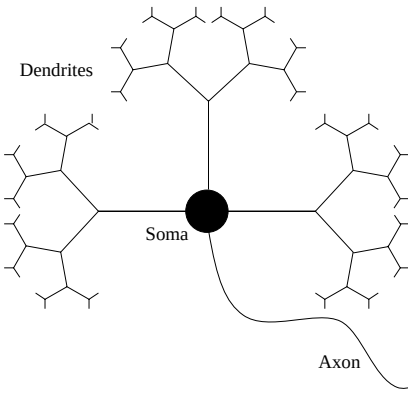

Fig. 1. Branching dendritic tree of an idealized single neuron.

Neurons display a wide range of dendritic morphology, ranging from compact arborizations to elaborate branching patterns. Those with large dendritic subunits have the potential for pseudo–independent computations to be performed simultaneously in distinct dendritic subregions[3]. Moreover, it has been suggested that there is a relationship between dendritic branching structure and neuronal firing patterns[4]. In the case of the visual system of the fly the way in which postsynaptic signals interact is essentially determined by the structure of the dendritic tree[5] and highlights the consequences of dendritic geometry for information processing. By virtue of its spatial extension, and its electrically passive nature, the dendritic tree can act as a spatio–temporal filter. It selects between specific temporal activations of spatially fixed synaptic inputs, since responses at the soma depend explicitly on the time for signals to diffuse along the branches of the tree. Furthermore, intrinsic modulation, say from background synaptic activity, can act to alter the cable properties of all or part of a dendritic tree, thereby changing its response to patterns of synaptic input. The recent interest in artificial neural networks[6,7,8] and single node network models ignores many of these aspects of dendritic organization. Dendritic branching and dendritic subunits[1], spatio–temporal patterns of synaptic contact[9,10], electrical properties of cell membrane[11,12], synaptic noise[13] and neuromodulation[14] all contribute to the computational power of a synaptic neural circuit. Importantly, the developmental changes in dendrites have been proposed as a mechanism for learning and memory.

In the absence of a theoretical framework it is not possible to test hypotheses relating to the functional significance of the dendritic tree. In this review, therefore, we exploit formal similarities between models of the dendritic tree and systems familiar to a theoretical physicist and describe, in a natural framework, the *physics of the extended neuron*. Our discussion ranges from the consequences of a diffusive structure, namely the dendritic tree, on the response of a single neuron, up to an

investigation of the properties of a neural field, describing an interacting population of neurons with dendritic structure. Contact with biological reality is maintained using established models of cell membrane in conjunction with realistic forms of nonlinear stochastic synaptic input.

A basic tenet underlying the description of a nerve fibre is that it is an electrical conductor[15]. The passive spread of current through this material causes changes in membrane potential. These current flows and potential changes may be described with a second–order linear partial differential equation essentially the same as that for flow of current in a telegraph line, flow of heat in a metal rod and the diffusion of substances in a solute. Hence, the equation as applied to nerve cells is commonly known as the *cable equation*. Rall[16] has shown how this equation can also represent an entire dendritic tree for the case of certain restricted geometries. In a later development he pioneered the idea of modelling a dendritic tree as a graph of connected electrical compartments[17]. In principle this approach can represent any arbitrary amount of nonuniformity in a dendritic branching pattern as well as complex compartment dependencies on voltage, time and chemical gradients and the space and time–dependent synaptic inputs found in biological neurons. Compartmental modelling represents a finite–difference approximation of a linear cable equation in which the dendritic system is divided into sufficiently small regions such that spatial variations of the electrical properties within a region are negligible. The partial differential equations of cable theory then simplify to a system of first–order ordinary differential equations. In practice a combination of matrix algebra and numerical methods are used to solve for realistic neuronal geometries[18,19].

In section 2, we indicate how to calculate the fundamental solution or Green's function of both the cable equation and compartmental model equation of an arbitrary dendritic tree. The Green's function determines the passive response arising from the instantaneous injection of a unit current impulse at a given point on the tree. In the case of the cable equation a path integral approach can be used, whereby the Green's function of the tree is expressed as an integral of a certain measure over all the paths connecting one point to another on the tree in a certain time. Boundary conditions define the measure. The procedure for the compartmental model is motivated by exploiting the intimate relationship between random walks and diffusion processes[20]. The space–discretization scheme yields matrix solutions that can be expressed analytically in terms of a sum over paths of a random walk on the compartmentalized tree. This approach avoids the more complicated path integral approach yet produces the same results in the continuum limit.

In section 3 we demonstrate the effectiveness of the compartmental approach in calculating the somatic response to realistic spatio–temporal synaptic inputs on the dendritic tree. Using standard cable or compartmental theory, the potential change at any point depends linearly on the injected input current. In practice, postsynaptic *shunting* currents are induced by localized conductance changes associated with specific ionic membrane channels. The resulting currents are generally not proportional to the input conductance changes. The conversion from conductance

changes to somatic potential response is a *nonlinear* process. The response function depends nonlinearly on the injected current and is no longer time–translation invariant. However, a Dyson equation may be used to express the full solution in terms of the bare response function of the model without shunting. In fact Poggio and Torre[21,22] have developed a theory of synaptic interactions based upon the Feynman diagrams representing terms in the expansion of this Dyson equation. The nonlinearity introduced by shunting currents can induce a space and time–dependent cell membrane decay rate. Such dependencies are naturally accommodated within the compartmental framework and are shown to favour a low output–firing rate in the presence of high levels of excitation.

Not surprisingly, modifications in the membrane potential time constant of a cell due to synaptic background noise can also have important consequences for neuronal firing rates. In section 4 we show that techniques from the study of disordered solids are appropriate for analyzing compartmental neuronal response functions with shunting in the presence of such noise. With a random distribution of synaptic background activity a mean–field theory may be constructed in which the steady state behaviour is expressed in terms of an ensemble–averaged single–neuron Green's function. This Green's function is identical to the one found in the tight–binding alloy model of excitations in a one–dimensional disordered lattice. With the aid of the coherent potential approximation, the ensemble average may be performed to determine the steady state firing rate of a neuron with dendritic structure. For the case of time–varying synaptic background activity drawn from some coloured noise process, there is a correspondence with a model of excitons moving on a lattice with random modulations of the local energy at each site. The dynamical coherent potential approximation and the method of partial cumulants are appropriate for constructing the average single–neuron Green's function. Once again we describe the effect of this noise on the firing–rate.

Neural network dynamics has received considerable attention within the context of associative memory, where a self–sustained firing pattern is interpreted as a memory state[7]. The interplay between learning dynamics and retrieval dynamics has received less attention[23] and the effect of dendritic structure on either or both has received scant attention at all. It has become increasingly clear that the introduction of simple, yet biologically realistic, features into point processor models can have a dramatic effect upon network dynamics. For example, the inclusion of signal communication delays in artificial neural networks of the Hopfield type can destabilize network attractors, leading to delay–induced oscillations via an Andronov–Hopf bifurcation[24,25]. Undoubtedly, the dynamics of neural tissue does not depend solely upon the interactions between neurons, as is often the case in artificial neural networks. The dynamics of the dendritic tree, synaptic transmission processes, communication delays and the active properties of excitable cell membrane all play some role. However, before an all encompassing model of neural tissue is developed one must be careful to first uncover the fundamental neuronal properties contributing to network behaviour. The importance of this issue is underlined when one recalls

that the basic mechanisms for central pattern generation in some simple biological systems, of only a few neurons, are still unclear[26,27,28]. Hence, theoretical modelling of neural tissue can have an immediate impact on the interpretation of neurophysiological experiments if one can identify pertinent model features, say in the form of length or time scales, that play a significant role in determining network behaviour. In section 5 we demonstrate that the effects of dendritic structure are consistent with the two types of synchronized wave observed in cortex. Synchronization of neural activity over large cortical regions into periodic standing waves is thought to evoke typical EEG activity[29] whilst travelling waves of cortical activity have been linked with epileptic seizures, migraine and hallucinations[30]. First, we generalise the standard graded response Hopfield model[31] to accomodate a compartmental dendritic tree. The dynamics of a recurrent network of compartmental model neurons can be formulated in terms of a set of coupled nonlinear scalar Volterra integro–differential equations. Linear stability analysis and bifurcation theory are easily applied to this set of equations. The effects of dendritic structure on network dynamics allows the possibility of oscillation in a symmetrically connected network of compartmental neurons. Secondly, we take the continuum limit with respect to both network and dendritic coordinates to formulate a dendritic extension of the isotropic model of nerve tissue[32,30,33]. The dynamics of pattern formation in neural field theories lacking dendritic coordinates has been strongly influenced by the work of Wilson and Cowan[34] and Amari[32,35]. Pattern formation is typically established in the presence of competition between short–range excitation and long–range inhibition, for which there is little anatomical or physiological support[36]. We show that the diffusive nature of the dendritic tree can induce a Turing–like instability, leading to the formation of stable spatial and time–periodic patterns of network activity, in the presence of more biologically realistic patterns of axo–dendritic synaptic connections. Spatially varying patterns can also be established along the dendrites and have implications for Hebbian learning[37]. A complimentary way of understanding the spatio–temporal dynamics of neural networks has come from the study of coupled map lattices. Interestingly, the dynamics of integrate–and–fire networks can exhibit patterns of spiral wave activity[38]. We finish this section by discussing the link between the neural field theoretic approach and the use of coupled map lattices using the *weak–coupling* transform developed by Kuramoto[39]. In particular, we analyze an array of *pulse*–coupled integrate–and–fire neurons with dendritic structure, in terms of a continuum of *phase*–interacting oscillators. For long range excitatory coupling the bifurcation from a synchronous state to a state of travelling waves is described.

2. The uniform cable

A nerve cable consists of a long thin, electrically conducting core surrounded by a thin membrane whose resistance to transmembrane current flow is much greater than that of either the internal core or the surrounding medium. Injected current can travel long distances along the dendritic core before a significant fraction leaks

out across the highly resistive cell membrane. Linear cable theory expresses conservation of electric current in an infinitesimal cylindrical element of nerve fibre. Let $V(\xi,t)$ denote the membrane potential at position ξ along a cable at time t measured relative to the resting potential of the membrane. Let $\overline{\tau}$ be the cell membrane time constant, D the diffusion constant and λ the membrane length constant. In fact $\overline{\tau}=RC$, $\lambda=\sqrt{aR/(2r)}$ and $D=\lambda^2/\overline{\tau}$, where C is the capacitance per unit area of the cell membrane, r the resistivity of the intracellular fluid (in units of resistance $\times$ length), the cell membrane resistance is R (in units of resistance $\times$ area) and a is the cable radius. In terms of these variables the basic uniform cable equation is

$$\frac{\partial V(\xi,t)}{\partial t}=-\frac{V(\xi,t)}{\overline{\tau}}+D\frac{\partial^2 V(\xi,t)}{\partial \xi^2}+I(\xi,t),\quad \xi\in\mathbb{R},\quad t\geq 0 \tag{1}$$

where we include the source term $I(\xi,t)$ corresponding to external input injected into the cable. In response to a unit impulse at ξ' at $t=0$ and taking $V(\xi,0)=0$ the dendritic potential behaves as $V(\xi,t)=G(\xi-\xi',t)$, where

$$\begin{aligned} G(\xi,t) &= \int_{-\infty}^{\infty}\frac{\mathrm{d}k}{2\pi}\mathrm{e}^{ik\xi}\mathrm{e}^{-(1/\overline{\tau}+Dk^2)t} &(2)\\ &= \frac{1}{\sqrt{4\pi Dt}}\mathrm{e}^{-t/\overline{\tau}}\mathrm{e}^{-\xi^2/(4Dt)} &(3)\end{aligned}$$

and $G(\xi,t)$ is the fundamental solution or Green's function for the cable equation with unbounded domain. It is positive, symmetric and satisfies

$$\begin{aligned} \int_{-\infty}^{\infty}\mathrm{d}\xi G(\xi,t) &= \mathrm{e}^{-t/\overline{\tau}} &(4)\\ G(\xi,0) &= \delta(\xi) &(5)\\ \left(\frac{\partial}{\partial t}+\frac{1}{\overline{\tau}}-D\frac{\partial^2}{\partial\xi^2}\right)G(\xi,t) &= 0 &(6)\\ \int_{-\infty}^{\infty}\mathrm{d}\xi_1 G(\xi_2-\xi_1,t_2-t_1)G(\xi_1-\xi_0,t_1-t_0) &= G(\xi_2-\xi_0,t_2-t_0) &(7)\end{aligned}$$

Equation (5) describes initial conditions, (6) is simply the cable equation without external input whilst (7) (with $t_2>t_1>t_0$) is a characteristic property of Markov processes. In fact it is a consequence of the convolution properties of Gaussian integrals and may be used to construct a path integral representation. By dividing time into an arbitrary number of intervals and using (7) the Green's function for the uniform cable equation may be written

$$G(\xi-\xi',t)=\int_{-\infty}^{\infty}\prod_{k=0}^{n-1}\frac{\mathrm{d}z_k\mathrm{e}^{-(t_{k+1}-t_k)/\overline{\tau}}}{\sqrt{4\pi D(t_{k+1}-t_k)}}\exp\left(-\frac{1}{4D}\sum_{j=0}^{n-1}\left(\frac{z_{j+1}-z_j}{t_{j+1}-t_j}\right)^2\right) \tag{8}$$

with $z_0=\xi'$, $z_n=\xi$. This gives a precise meaning to the symbolic formula

$$G(\xi-\xi',t)=\int_{z(0)=\xi'}^{z(t)=\xi}\mathcal{D}\mathbf{z}(t')\exp\left(-\frac{1}{4D}\int_0^t\mathrm{d}t'\dot{\mathbf{z}}^2\right) \tag{9}$$

where $\mathcal{D}\mathbf{z}(t)$ implies integrals on the positions at intermediate times, normalised as in (8).

In the compartmental modelling approach an unbranched cylindrical region of a passive dendrite is represented as a linked chain of equivalent circuits as shown in figure 2. Each compartment consists of a membrane leakage resistor R_α in parallel with a capacitor C_α, with the ground representing the extracellular medium (assumed to be isopotential). The electrical potential $V_\alpha(t)$ across the membrane is measured with respect to some resting potential. The compartment is joined to its immediate neighbours in the chain by the junctional resistors $R_{\alpha,\alpha-1}$ and $R_{\alpha,\alpha+1}$. All parameters are equivalent to those of the cable equation, but restricted to individual compartments. The parameters C_α, R_α and $R_{\alpha\beta}$ can be related to the underlying membrane properties of the dendritic cylinder as follows. Suppose that the cylinder has uniform diameter d and denote the length of the α^{th} compartment by l_α. Then

$$C_\alpha = c_\alpha l_\alpha \pi d, \quad R_\alpha = \frac{1}{g_\alpha l_\alpha \pi d}, \quad R_{\alpha\beta} = \frac{2r_\alpha l_\alpha + 2r_\beta l_\beta}{\pi d^2} \tag{10}$$

where g_α and c_α are the membrane conductance and capacitance per unit area, and r_α is the longitudinal resistivity. An application of Kirchoff's law to a compartment shows that the total current through the membrane is equal to the difference between the longitudinal currents entering and leaving that compartment. Thus,

$$C_\alpha \frac{\mathrm{d}V_\alpha}{\mathrm{d}t} = -\frac{V_\alpha}{R_\alpha} + \sum_{<\beta;\alpha>} \frac{V_\beta - V_\alpha}{R_{\alpha\beta}} + I_\alpha(t), \quad t \geq 0 \tag{11}$$

where $I_\alpha(t)$ represents the net external input current into the compartment and $<\beta;\alpha>$ indicates that the sum over β is restricted to immediate neighbours of α. Dividing through by C_α (and absorbing this factor within the $I_\alpha(t)$), equation (11) may be written as a linear matrix equation[18]:

$$\frac{\mathrm{d}\mathbf{V}}{\mathrm{d}t} = \mathbf{Q}\mathbf{V} + \mathbf{I}(t), \quad Q_{\alpha\beta} = -\frac{\delta_{\alpha,\beta}}{\tau_\alpha} + \sum_{<\beta';\alpha>} \frac{\delta_{\beta,\beta'}}{\tau_{\alpha\beta'}} \tag{12}$$

where the membrane time constant τ_α and junctional time constant $\tau_{\alpha\beta}$ are

$$\frac{1}{\tau_\alpha} = \frac{1}{C_\alpha}\left[\sum_{<\beta';\alpha>} \frac{1}{R_{\alpha\beta'}} + \frac{1}{R_\alpha}\right], \quad \frac{1}{\tau_{\alpha\beta}} = \frac{1}{C_\alpha R_{\alpha\beta}} \tag{13}$$

Equation (12) may be formally solved as

$$V_\alpha(t) = \sum_\beta \int_0^t \mathrm{d}t' G_{\alpha\beta}(t-t') I_\beta(t') + \sum_\beta G_{\alpha\beta}(t) V_\beta(0), \quad t \geq 0 \tag{14}$$

with

$$G_{\alpha\beta}(t) = \left[\mathrm{e}^{\mathbf{Q}t}\right]_{\alpha\beta} \tag{15}$$

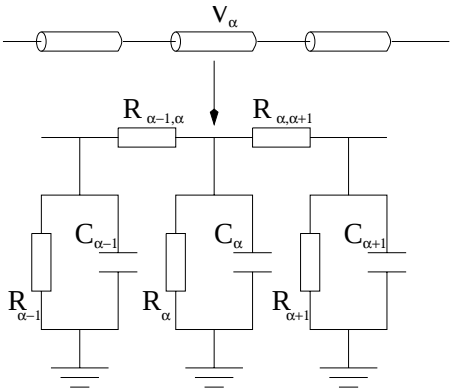

Fig. 2. Equivalent circuit for a compartmental model of a chain of successive cylindrical segments of passive dendritic membrane.

The response function $G_{\alpha\beta}(T)$ determines the membrane potential of compartment α at time t in response to a unit impulse stimulation of compartment β at time $t-T$. The matrix $\mathbf{Q}$ has real, negative, nondegenerate eigenvalues λ_r reflecting the fact that the dendritic system is described in terms of a passive RC circuit, recognized as a dissipative system. Hence, the response function can be obtained by diagonalizing $\mathbf{Q}$ to obtain $G_{\alpha\beta}(t) = \sum_r C^r_{\alpha\beta} \mathrm{e}^{-|\lambda_r|t}$ for constant coefficients determined, say, by Sylvester's expansion theorem. We avoid this cumbersome approach and instead adopt the recent approach due to Bressloff and Taylor[40].

For an infinite uniform chain of linked compartments we set $R_\alpha = R$, $C_\alpha = C$ for all α, $R_{\alpha\beta} = R_{\beta\alpha} = R'$ for all $\alpha = \beta + 1$ and define $\overline{\tau} = RC$ and $\gamma = R'C$. Under such assumptions one may write

$$Q_{\alpha\beta} = -\frac{\delta_{\alpha,\beta}}{\tau} + \frac{K_{\alpha\beta}}{\gamma}, \quad \frac{1}{\tau} = \frac{1}{\overline{\tau}} + \frac{2}{\gamma}. \tag{16}$$

The matrix $\mathbf{K}$ generates paths along the tree and in this case is given by

$$K_{\alpha\beta} = \delta_{\alpha-1,\beta} + \delta_{\alpha+1,\beta} \tag{17}$$

The form (16) of the matrix $\mathbf{Q}$ carries over to dendritic trees of arbitrary topology provided that each branch of the tree is uniform and certain conditions are imposed on the membrane properties of compartments at the branching nodes and terminals of the tree[40]. In particular, modulo additional constant factors arising from the boundary conditions at terminals and branching nodes $[\mathbf{K}^m]_{\alpha\beta}$ is equal to the number of possible paths consisting of m steps between compartments α and β (with possible reversals of direction) on the tree, where a step is a single jump between neighbouring compartments. Thus calculation of $G_{\alpha\beta}(t)$ for an arbitrary branching geometry reduces to (i) determining the sum over paths $[\mathbf{K}^m]_{\alpha\beta}$, and

then (ii) evaluating the following series expansion of $\mathrm{e}^{\mathbf{Q}t}$,

$$G_{\alpha\beta}(t) = \mathrm{e}^{-t/\tau} \sum_{m\geq 0} \left(\frac{t}{\gamma}\right)^m \frac{1}{m!} \left[\mathbf{K}^m\right]_{\alpha\beta} \tag{18}$$

The global factor $\mathrm{e}^{-t/\tau}$ arises from the diagonal part of $\mathbf{Q}$.

For the uniform chain, the number of possible paths consisting of m steps between compartments α and β can be evaluated using the theory of random walks[41],

$$\left[\mathbf{K}^m\right]_{\alpha\beta} = N_0[|\alpha-\beta|, m] \tag{19}$$

where

$$N_0[L, m] = \binom{m}{[m+L]/2} \tag{20}$$

The response function of the chain (18) becomes

$$\begin{aligned} G_{\alpha\beta}(t) &= \mathrm{e}^{-t/\tau} \sum_{m\geq 0} \left(\frac{t}{\gamma}\right)^{2m+|\beta-\alpha|} \frac{1}{(m+|\beta-\alpha|)!m!} &(21)\\ &= \mathrm{e}^{-t/\tau} I_{|\beta-\alpha|}(2t/\gamma) &(22)\end{aligned}$$

where $I_n(t)$ is a modified Bessel function of integer order n. Alternatively, one may use the fact that the response function $G_{\alpha\beta}(t)$ satisfies

$$\frac{\mathrm{d}G_{\alpha\beta}}{\mathrm{d}t} = \sum_{\gamma} Q_{\alpha\gamma} G_{\gamma\beta}, \quad G_{\alpha\beta}(0) = \delta_{\alpha,\beta} \tag{23}$$

which may be solved using Fourier transforms, since for the infinite chain $G_{\alpha\beta}(t)$ depends upon $|\alpha-\beta|$ (translation invariance). Thus

$$G_{\alpha\beta}(t) = \int_{-\pi}^{\pi} \frac{\mathrm{d}k}{2\pi} \mathrm{e}^{ik|\alpha-\beta|} \mathrm{e}^{-\epsilon(k)t} \tag{24}$$

where

$$\epsilon(k) = \tau^{-1} - 2\gamma^{-1}\cos k \tag{25}$$

Equation (24) is the well known integral representation of equation (22). The response function (22) is plotted as a function of time (in units of γ) in figure 3 for a range of separations $m = \alpha - \beta$. Based on typical values of membrane properties[18] we take γ = 1msec and $\overline{\tau} = 10\gamma$. The response curves of figure 3 are similar to those found in computer simulations of more detailed model neurons[19]; that is, the simple analytical expression, equation (22), captures the essential features of the effects of the passive membrane properties of dendrites. In particular the sharp rise to a large peak, followed by a rapid early decay in the case of small separations, and

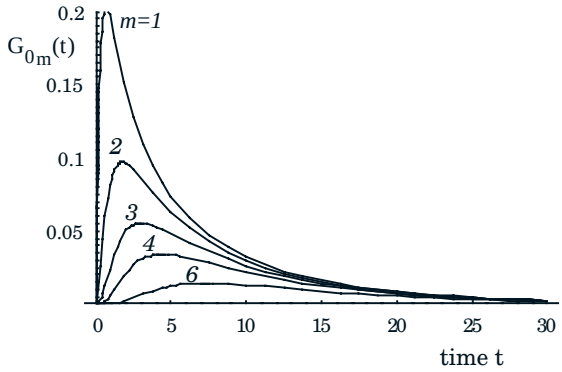

Fig. 3. Response function of an infinite chain as a function of t (in units of γ) with $\overline{\tau} = 10\gamma$ for various values of the separation distance m.

the slower rise to a later and more rounded peak for larger separations is common to both analyses.

A re–labelling of each compartment by its position along the dendrite as $\xi = l\alpha$, $\xi' = l\beta$, $\alpha, \beta = 0 \pm 1, \pm 2, \ldots$, with l the length of an individual compartment makes it easy to take the continuum limit of the above model. Making a change of variable $k \to k/l$ on the right hand side of (24) and taking the continuum limit $l \to 0$ gives

$$G(\xi - \xi', t) = \mathrm{e}^{-t/\overline{\tau}} \lim_{l \to 0} \int_{-\pi/l}^{\pi/l} \frac{\mathrm{d}k}{2\pi} \mathrm{e}^{ik(\xi - \xi')} \mathrm{e}^{-[k^2 l^2 t/\gamma + \ldots]} \tag{26}$$

which reproduces the fundamental result (3) for the standard cable equation upon taking $D = \lim_{l \to 0} l^2/\gamma$.

An arbitrary dendritic tree may be construed as a set of branching nodes linked by finite length pieces of nerve cable. In a sense, the fundamental building blocks of a dendritic tree are compartmental chains plus encumbant boundary conditions and single branching nodes. Rall[42] has described the conditions under which a branched tree is equivalent to an infinite cable. From the knowledge of boundary conditions at branching nodes, a tree geometry can be specified such that all junctions are impedance matched and injected current flows without reflection at these points. The statement of Rall's *3/2* power law for equivalent cylinders has the particularly simple geometric expression that $d_p^{3/2} = \sum d_d^{3/2}$ where d_p (d_d) is the diameter of the parent (daughter) dendrite. Analytic solutions to the multicylinder cable model may be found in[43] where a nerve cell is represented by a set of equivalent cylinders. A more general analysis for arbitrary branching dendritic geometries, where each branch is described by a one–dimensional cable equation, can be generated by a graphical calculus developed in[44], or using a path–integral method based on equation (8)[45,46]. The results of the path–integral approach are most easily understood in terms of an equivalent compartmental formulation based on equation

(18)[40]. For an arbitrary granching geometry, one can exploit various reflection arguments from the theory of random walks[41] to express $[\mathbf{K}^m]_{\alpha\beta}$ of equation (18) in the form $\sum_{\mu}^{(\alpha,\beta)} c_\mu N_0[L_\mu, m]$. This summation is over a restricted class of paths (or *trips*) μ of length L_μ from α to β on a corresponding uniform infinite dendritic chain. It then follows from equations (21) and (22) that the Green's function on an arbitrary tree can be expressed in the form $G_{\alpha\beta}(t) = \sum_{\mu}^{(\alpha,\beta)} c_\mu I_{L_\mu}(2t/\gamma)$. Explicit rules for calculating the appropriate set of trips together with the coefficients c_μ are given elsewhere[47]. Finally, the results of the path–integral approach are recovered by taking the continuum limit of each term in the sum–over–trips using equation (26). The sum–over–trips representation of the Green's function on a tree is particularly suited for determining short–time response, since one can then truncate the (usually infinite) series to include only the shortest trips. Laplace transform techniques developed by Bressloff *et al*[47] also allow explicit construction of the long–term response.

The role of spatial structure in temporal information processing can be clarified with the aid of equation (14), assuming $V_\alpha(0) = 0$ for simplicity. Taking the soma to be the compartment labelled by $\alpha = 0$ the response at the cell body to an input of the form $I_\alpha(t) = w_\alpha I(t)$ is

$$V_0(t) = \sum_\beta w_\beta \hat{I}_\beta(t) \tag{27}$$

where $\hat{I}_\beta(t) = \int_0^t \mathrm{d}t' G_{0\beta}(t-t')I(t')$. Regarding w_α as a weight and $I(t)$ as a time–varying input signal, the compartmental neuron acts as a perceptron[48] with an input layer of linear filters that transforms the original signal $I(t)$ into a set of signals $\hat{I}_\alpha(t)$. The filtered signal is obtained with a convolution of the compartmental response function $G_{0\beta}(t)$. Thus the compartmental neuron develops over time a set of memory traces of previous input history from which temporal information can be extracted. Applications of this model to the storage of temporal sequences are detailed in[49]. If the weighting function w_α has a spatial component as $w_\alpha = w\cos p\alpha$ then, making use of the fact that the Fourier transform of $G_{\alpha\beta}(t)$ is given from (24) as $\mathrm{e}^{-\epsilon(k)t}$ and that $\epsilon(k) = \epsilon(-k)$, the somatic response becomes

$$V_0(t) = w\int_0^t \mathrm{d}t' \mathrm{e}^{-\epsilon(p)(t-t')} I(t') \tag{28}$$

For a simple pulsed input signal $I(t) = \delta(t)$ the response is characterised by a decaying exponential with the rate of decay given by $\epsilon(p)$. Taking $\overline{\tau} \gg \gamma$ the decay rate $\epsilon(p)$ is dominated by the p dependent term $2(1-\cos p)/\gamma$. When $p = 0$ the membrane potential $V_0(t)$ decays slowly with rate $1/\overline{\tau}$. On the other hand with $p = \pi$, $V_0(t)$ decays rapidly with rate $4/\gamma$. The dependence of decay rates on the spatial frequency of excitations is also discussed for the cable equation using Fourier methods by Rall[50].

To complete the description of a compartmental model neuron, a firing mechanism must be specified. A full treatment of this process requires a detailed description of the interactions between ionic currents and voltage dependent channels in the

soma (or more precisely the axon hillock) of the neuron. When a neuron fires there is a rapid depolarization of the membrane potential at the axon hillock followed by a hyperpolarization due to delayed potassium rectifier currents. A common way to represent the firing history of a neuron is to regard neuronal firing as a threshold process. In the so–called *integrate–and–fire* model, a firing event occurs whenever the somatic potential exceeds some threshold. Subsequently, the membrane potential is immediately reset to some resting level. The dynamics of such integrate-and–fire models lacking dendritic structure has been extensively investigated[51,52,53,54]. Rospars and Lansky[55] have tackled a more general case with a compartmental model in which it is assumed that dendritic potentials evolve without any influence from the nerve impulse generation process. However, a model with an active (integrate–and–fire) compartment coupled to a passive compartmental tree can be analyzed explicitly without this dubious assumption. In fact the electrical coupling between the soma and dendrites means that there is a feedback signal across the dendrites whenever the somatic potential resets. This situation is described in detail by Bressloff[56]. The basic idea is to eliminate the passive component of the dynamics (the dendritic potential) to yield a Volterra integro–differential equation for the somatic potential. An iterative solution to the integral equation can be constructed in terms of a second–order map of the firing times, in contrast to a first order map as found in point–like models. We return again to the interesting dynamical aspects associated with integrate–and–fire models with dendritic structure in section 5.

3. Synaptic interactions in the presence of shunting currents

Up till now the fact that changes in the membrane potential $V(\xi,t)$ of a nerve cable induced by a synaptic input at ξ depend upon the size of the deviation of $V(\xi,t)$ from some resting potential has been ignored. This biologically important phenomenon is known as *shunting*. If such shunting effects are included within the cable equation then the synaptic input current $I(\xi,t)$ of equation (1) becomes $V(\xi,t)$ dependent. The postsynaptic current is in fact mainly due to localized conductance changes for specific ions, and a realistic form for it is

$$I(\xi,t)=\Gamma(\xi,t)[S-V(\xi,t)] \tag{29}$$

where $\Gamma(\xi,t)$ is the conductance change at location ξ due to the arrival of a presynaptic signal and S is the effective membrane reversal potential associated with all the ionic channels. Hence, the postsynaptic current is no longer simply proportional to the input conductance change. The cable equation is once again given by (1) with $\overline{\tau}^{-1}\rightarrow\overline{\tau}^{-1}+\Gamma(\xi,t)\equiv Q(\xi,t)$ and $I(\xi,t)\equiv S\Gamma(\xi,t)$. Note the spatial and temporal dependence of the cell membrane decay function $Q(\xi,t)$. The membrane potential can still be written in terms of a Green's function as

$$V(\xi,t)=\int_0^t \mathrm{d}s\int_{-\infty}^{\infty}\mathrm{d}\xi' G(\xi-\xi';t,s)I(\xi',s)+\int_{-\infty}^{\infty}\mathrm{d}\xi' G(\xi-\xi';t,0)V(\xi',0) \tag{30}$$

but now the Green's function depends on s and t independently and is no longer

time–translation invariant. Using the n fold convolution identity for the Green's function we may write it in the form

$$G(\xi-\xi';t,s)=\prod_{j=1}^{n-1}\int_{-\infty}^{\infty}\mathrm{d}z_j G(\xi-z_1;t,t_1)G(z_1-z_2;t_1,t_2)\dots G(z_{n-1}-\xi';t_{n-1},s) \tag{31}$$

This is a particularly useful form for the analysis of spatial and temporal varying cell membrane decay functions induced by the shunting current. For large n the Green's function $G(\xi-\xi';t,s)$ can be approximated by an n fold convolution of approximations to the short time Green's function $G(z_j-z_{j+1};t_j,t_{j+1})$. Motivated by results from the analysis of the cable equation in the absence of shunts it is natural to try

$$G(z_j-z_{j+1};t_j,t_{j+1})\approx \mathrm{e}^{-\frac{(t_{j+1}-t_j)}{2}(\Gamma(z_j,t_j)+\Gamma(z_{j+1},t_{j+1}))}G(z_j-z_{j+1},t_{j+1}-t_j) \tag{32}$$

where $G(\xi,t)$ is the usual Green's function for the cable equation with unbounded domain and the cell membrane decay function is approximated by its spatio–temporal average. Substituting this into (31) and taking the limit $n\to\infty$ gives the result

$$G(\xi-\xi';t,s)=\lim_{n\to\infty}\prod_{j=1}^{n-1}\int_{-\infty}^{\infty}\mathrm{d}z_j \mathrm{e}^{-\frac{\Delta t}{2}\Gamma(\xi,t)}G(\xi-z_1,\Delta t)$$
$$\times\mathrm{e}^{-\Delta t\Gamma(z_1,t-\Delta t)}G(z_1-z_2,\Delta t)\mathrm{e}^{-\Delta t\Gamma(z_2,t-2\Delta t)}\dots G(z_{n-1}-\xi',\Delta t)\mathrm{e}^{-\frac{\Delta t}{2}\Gamma(\xi',s)} \tag{33}$$

where $\Delta t=(t-s)/n$. The heuristic method for calculating such path–integrals is based on a rule for generating random walks. Paths are generated by starting at the point ξ and taking n steps of length $\sqrt{2D\Delta t}$ choosing at each step to move in the positive or negative direction along the cable with probability $1/2\times$ an additional weighting factor. For a path that passes through the sequence of points $\xi\to z_1\to z_2\dots\to\xi'$ this weighting factor is given by

$$W(\xi\to z_1\to z_2\dots\to\xi')=\mathrm{e}^{-\Delta t\left(\frac{1}{2}\Gamma(\xi,t)+\Gamma(z_1,t-\Delta t)+\dots+\frac{1}{2}\Gamma(\xi',s)\right)} \tag{34}$$

The normalized distribution of final points ξ' achieved in this manner will give the Green's function (33) in the limit $n\to\infty$. If we independently generate p paths of n steps all starting from the point x then

$$G(\xi-\xi';t,s)=\lim_{n\to\infty}\lim_{p\to\infty}\frac{1}{p}\sum_{\xi\to\xi'}^{paths}W(\xi\to z_1\to z_2\dots\to\xi') \tag{35}$$

It can be shown that this procedure does indeed give the Green's function satisfying the cable equation with shunts[45]. For example, when the cell membrane decay function only depends upon t such that $Q(\xi,t)=\overline{\tau}^{-1}+\Gamma(t)$ then using (33), and taking the limit $\Delta t\to 0$, the Green's function simply becomes

$$G(\xi-\xi';t,s)=\exp(-\int_s^t \mathrm{d}t'\Gamma(t'))G(\xi-\xi',t-s) \tag{36}$$

as expected, where $G(\xi, t)$ on the right hand side of (36) satisfies the cable equation on an unbounded domain given by equation (6).

To incorporate shunting effects into the compartmental model described by (11) we first examine in more detail the nature of synaptic inputs. The arrival of an action potential at a synapse causes a depolarisation of the presynaptic cell membrane resulting in the release of packets of neurotransmitters. These drift across the synaptic cleft and bind with a certain efficiency to receptors on the postsynaptic cell membrane. This leads to the opening and closing of channels allowing ions $(\mathrm{Na}^+, \mathrm{K}^+, \mathrm{Cl}^-)$ to move in and out of the cell under concentration and potential gradients. The ionic membrane current is governed by a time–varying conductance in series with a reversal potential S whose value depends on the particular set of ions involved. Let $\Delta g_{\alpha k}(t)$ and $S_{\alpha k}$ denote, respectively, the increase in synaptic conductance and the membrane reversal potential associated with the k^{th} synapse of compartment α, with $k = 1, \ldots P$. Then the total synaptic current is given by

$$\sum_{k=1}^{P} \Delta g_{\alpha k}(t)[S_{\alpha k} - V_\alpha(t)] \tag{37}$$

Hence, an infinite chain of compartments with shunting currents can be written

$$\frac{\mathrm{d}\mathbf{V}}{\mathrm{d}t} = \mathbf{H}(t)\mathbf{V} + \mathbf{I}(t), \quad t \geq 0 \tag{38}$$

where $\mathbf{H}(t) = \mathbf{Q} + \overline{\mathbf{Q}}(t)$ and

$$\overline{Q}_{\alpha\beta}(t) = -\frac{\delta_{\alpha,\beta}}{C_\alpha} \sum_k \Delta g_{\alpha k}(t) \equiv -\delta_{\alpha,\beta}\Gamma_\alpha(t), \quad I_\alpha(t) = \frac{1}{C_\alpha} \sum_k \Delta g_{\alpha k}(t) S_{\alpha k} \tag{39}$$

Formally, equation (38) may be solved as

$$V_\alpha(t) = \int_0^t \mathrm{d}t' \sum_\beta G_{\alpha\beta}(t, t') I_\beta(t') + \sum_\beta G_{\alpha\beta}(t, 0) V(0) \tag{40}$$

with

$$G_{\alpha\beta}(t, s) = \mathbf{T}\left[\exp\left(\int_s^t \mathrm{d}t' \mathbf{H}(t')\right)\right]_{\alpha\beta} \tag{41}$$

where $\mathbf{T}$ denotes the time–ordering operator, that is $\mathbf{T}[\mathbf{H}(t)\mathbf{H}(t')] = \mathbf{H}(t)\mathbf{H}(t')\Theta(t - t') + \mathbf{H}(t')\mathbf{H}(t)\Theta(t' - t)$ where $\Theta(x) = 1$ for $x \geq 0$ and $\Theta(x) = 0$ otherwise. Note that, as in the continuum case, the Green's function is no longer time–translation invariant. Poggio and Torre have pioneered a different approach to solving the set of equations (38) in terms of Volterra integral equations[21,22]. This leads to an expression for the response function in the form of a Dyson–like equation,

$$G_{\alpha\beta}(t, t') = G_{\alpha\beta}(t - t') - \int_{t'}^t \mathrm{d}t'' \sum_\gamma G_{\alpha\gamma}(t - t'')\Gamma_\gamma(t'')G_{\gamma\beta}(t'', t') \tag{42}$$

where $G_{\alpha\beta}(t)$ is the response function without shunting. The right–hand side of (42) may be expanded as a Neumann series in $\Gamma_\alpha(t)$ and $G_{\alpha\beta}(t)$, which is a bounded, continuous function of t. Poggio and Torre exploit the similarity between the Neumann expansion of (42) and the S–matrix expansion of quantum field theory. Both are solutions of linear integral equations; the linear kernel is in one case the Green's function $G_{\alpha\beta}(t)$ (or $G(\xi,t)$ for the continuum version), in the other case the interaction Hamiltonian. In both approaches the iterated kernels of higher order obtained through the recursion of (42) are dependent solely upon knowledge of the linear kernel. Hence, the solution to the linear problem can determine uniquely the solution to the full nonlinear one. This analogy has led to the implementation of a graphical notation similar to Feynman diagrams that allows the construction of the somatic response in the presence of shunting currents. In practice the convergence of the series expansion for the full Green's function is usually fast and the first few terms (or graphs) often suffice to provide a satisfactory approximation. Moreover, it has been proposed that a full analysis of a branching dendritic tree can be constructed in terms of such Feynman diagrams[21,22]. Of course, for branching dendritic geometries, the fundamental propagators or Green's functions on which the full solution is based will depend upon the geometry of the tree[40].

In general the form of the Green's function (41) is difficult to analyze due to the time–ordering operator. It is informative to examine the special case when i) each post–synaptic potential is idealised as a Dirac–delta function, ie details of the synaptic transmission process are neglected and ii) the arrival times of signals are restricted to integer multiples of a fundamental unit of time t_D. The time varying conductance $\Delta g_{\alpha k}(t)$ is then given by a temporal sum of spikes with the form

$$\Delta g_{\alpha k}(t) = \epsilon_{\alpha k} \sum_{m\geq 0} \delta(t - mt_D) a_{\alpha k}(m) \tag{43}$$

where $a_{\alpha k}(m) = 1$ if a signal (action potential) arrives at the discrete time mt_D and is zero otherwise. The size of each conductance spike, $\epsilon_{\alpha k}$, is determined by factors such as the amount of neurotransmitter released on arrival of an action potential and the efficiency with which these neurotransmitters bind to receptors. The terms defined in (39) become

$$\overline{Q}_{\alpha\beta}(t) = -\delta_{\alpha\beta} \sum_{m\geq 0} \delta(t - mt_D) q_\alpha(m), \quad I_\alpha(t) = \sum_{m\geq 0} \delta(t - mt_D) u_\alpha(m) \tag{44}$$

$$q_\alpha(m) = \sum_k \epsilon_{\alpha k} a_{\alpha k}(m), \quad u_\alpha(m) = \sum_k \epsilon_{\alpha k} S_{\alpha k} a_{\alpha k}(m) \tag{45}$$

and for convenience the capacitance C_α has been absorbed into each $\epsilon_{\alpha k}$ so that $\epsilon_{\alpha k}$ is dimensionless.

The presence of the Dirac–delta functions in (43) now allows the integrals in the formal solution (40) to be performed explicitly. Substituting (44) into (40) with

$t_D = 1$ and setting $V_\alpha(0) = 0$, we obtain for non–integer times t,

$$V_\alpha(t) = \sum_\beta \sum_{n=0}^{[t]} \mathbf{T} \left[\exp\left(\int_n^{t'} \mathrm{d}t' \left\{ \mathbf{Q} - \sum_{p\geq 0} \tilde{\mathbf{Q}}(p)\delta(t'-p) \right\} \right) \right]_{\alpha\beta} u_\beta(n) \qquad (46)$$

where $[t]$ denotes the largest integer $m \leq t$, $\tilde{Q}_{\alpha\beta}(p) = \delta_{\alpha,\beta} q_\alpha(p)$ and $u_\alpha(n)$ and $q_\alpha(n)$ are given in (45). The time–ordered product in (46) can be evaluated by splitting the interval $[n,[t]]$ into LT equal partitions $[t_i, t_{i+1}]$, where $T = [t] - n$, $t_0 = n$, $t_L = n+1, \ldots, t_{LT} = [t]$, such that $\delta(t-s) \to \delta_{i,Ls}/L$. In the limit $L \to \infty$, we obtain

$$V_\alpha(t) = \sum_\beta \sum_{n=0}^{[t]} \left(\left[\mathrm{e}^{(t-[t])\mathbf{Q}} \mathrm{e}^{-\tilde{\mathbf{Q}}([t])} \mathrm{e}^{\mathbf{Q}} \mathrm{e}^{-\tilde{\mathbf{Q}}([t]-1)} \ldots \mathrm{e}^{\mathbf{Q}} \mathrm{e}^{-\tilde{\mathbf{Q}}(n)} \right]_{\alpha\beta} \right) u_\beta(n) \qquad (47)$$

which is reminiscent of the path–integral equation (33) for the continuous cable with shunts. Equation (47) may be rewritten as

$$V_\alpha(t) = \sum_\beta \left[\mathrm{e}^{(t-m)\mathbf{Q}} \mathrm{e}^{-\tilde{\mathbf{Q}}(m)} \right]_{\alpha\beta} X_\beta(m) \qquad (48)$$

$$X_\alpha(m) = \sum_\beta \left[\mathrm{e}^{\mathbf{Q}} \mathrm{e}^{-\tilde{\mathbf{Q}}(m-1)} \right]_{\alpha\beta} X_\beta(m-1) + u_\alpha(m), \quad m < t < m+1 \qquad (49)$$

with $X_\alpha(m)$ defined iteratively according to (49) and $X_\alpha(0) = u_\alpha(0)$. The main effect of shunting is to alter the local decay rate of a compartment as $\tau^{-1} \to \tau^{-1} + q_\alpha(m)/(t-m)$ for $m < t \leq m+1$.

The effect of shunts on the steady–state $X_\alpha^\infty = \lim_{m\to\infty} X_\alpha(m)$ is most easily calculated in the presence of constant synaptic inputs. For clarity, we consider two groups of identical synapses on each compartment, one excitatory and the other inhibitory with constant activation rates. We take $S_{\alpha k} = S^{(e)}$ for all excitatory synapses and $S_{\alpha k} = 0$ for all inhibitory synapses (shunting inhibition). We also set $\epsilon_{\alpha k} = 1$ for all α, k. Thus equation (45) simplifies to

$$q_\alpha = E_\alpha + \overline{E}_\alpha, \quad u_\alpha = S^{(e)} E_\alpha \qquad (50)$$

where E_α and $\overline{E}_\alpha$ are the total rates of excitation and inhibition for compartment α. We further take the pattern of input stimulation to be non–recurrent inhibition of the form (see figure 4):

$$E_\alpha = a_\alpha E, \quad \sum_\beta a_\beta = 1, \quad \overline{E}_\alpha = \sum_{\beta\neq\alpha} E_\alpha \qquad (51)$$

An input that excites the α^{th} compartment also inhibits all other compartments in the chain. The pattern of excitation across the chain is completely specified by the a_α's. The steady state X_α^∞ is

$$X_\alpha^\infty = S^{(e)} E \lim_{m\to\infty} \sum_{n=0}^{m} \sum_\beta a_\beta \exp\left(-n \left(\frac{1}{\tau} + E \right) \right) I_{|\beta-\alpha|}(2n/\gamma) \qquad (52)$$

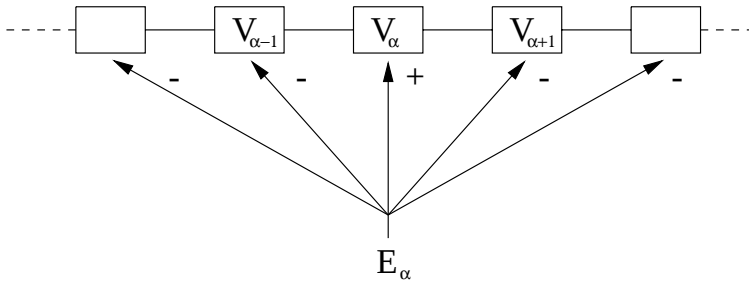

Fig. 4. Non–recurrent inhibition

and we have made use of results from section 2, namely equations (16) and (22). The series on the right hand side of (52) is convergent so that the steady–state X_α^∞ is well defined. Note that X_α^∞ determines the long–term behaviour of the membrane potentials according to equation (48). For small levels of excitation E, X_α^∞ is approximately a linear function of E. However, as E increases, the contribution of shunting inhibition to the effective decay rate becomes more significant. Eventually X_α^∞ begins to decrease.

Finally, using parallel arguments to Abbott[57] it can be shown that the nonlinear relationship between X_α^∞ and E in equation (52) provides a solution to the problem of high neuronal firing–rates. A reasonable approximation to the *average* firing rate Ω of a neuron is[58]

$$\Omega = f(X_0^\infty(E)) = \frac{f_{\max}}{1 + \exp(g[h - X_0^\infty(E)])} \tag{53}$$

for some gain g and threshold h where $f_{\max}$ is the maximum firing rate. Consider a population of excitatory neurons in which the effective excitatory rate E impinging on a neuron is determined by the average firing rate $\langle\Omega\rangle$ of the population. For a large population of neurons a reasonable approximation is to take $E = c\langle\Omega\rangle$ for some constant c. Within a mean–field approach, the steady state behaviour of the population is determined by the self–consistency condition $E = cf(X_0^\infty(E))$[57]. Graphical methods show that there are two stable solutions, one corresponding to the quiescent state with $E = 0$ and the other to a state in which the firing–rate is considerably below $f_{\max}$. In contrast, if X_0^∞ were a linear function of E then this latter stable state would have a firing–rate close to $f_{\max}$, which is not biologically realistic. This is illustrated in figure 5 for $a_\beta = \delta_{\beta,1}$.

4. Effects of background synaptic noise

Neurons typically possess up to 10^5 synapses on their dendritic tree. The spontaneous release of neurotransmitter into such a large number of clefts can substantially alter spatio–temporal integration in single cells[59,60]. Moreover, one would expect consequences for such *background synaptic noise* on the firing rates of neuronal

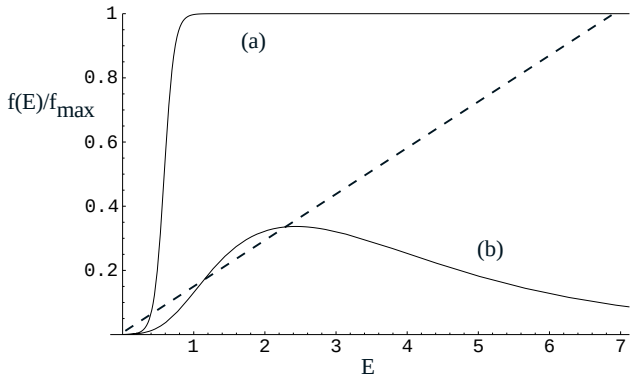

Fig. 5. Firing–rate/maximum firing rate $f/f_{\max}$ as a function of input excitation E for (a) linear and (b) nonlinear relationship between steady–state membrane potential X_0^∞ and E. Points of intersection with straight line are states of self–sustained firing.

populations. Indeed, the absence of such noise for *in–vitro* preparations, without synaptic connections, allows experimental determination of the effects of noise upon neurons *in–vivo*. In this section we analyse the effects of random synaptic activity on the steady–state firing rate of a compartmental model neural network with shunting currents. In particular we calculate firing–rates in the presence of random noise using techniques from the theory of disordered media and discuss the extension of this work to the case of time–varying background activity.

Considerable simplification of time–ordered products occurs for the case of constant input stimulation. Taking the input to be the pattern of non–recurrent inhibition given in section 3, the formal solution for the compartmental shunting model (40), with $V_\alpha(0) = 0$ reduces to

$$V_\alpha(t) = \sum_\beta \int_0^t \mathrm{d}t' \widehat{G}_{\alpha\beta}(t-t') I_\beta(t'), \quad \widehat{G}_{\alpha\beta}(t) = \left[\mathrm{e}^{(\mathbf{Q}-\widetilde{\mathbf{Q}})t}\right]_{\alpha\beta} \tag{54}$$

where $\widetilde{Q}_{\alpha\beta} = (E_\alpha + \overline{E}_\alpha)\delta_{\alpha,\beta}$ and $I_\alpha = S^{(e)}E_\alpha$. The background synaptic activity impinging on a neuron residing in a network introduces some random element for this stimulus. Consider the case for which the background activity contributes to the inhibitory rate $\overline{E}_\alpha$ in a simple additive manner so that

$$\overline{E}_\alpha = \sum_{\beta\neq\alpha} E_\beta + \eta_\alpha \tag{55}$$

Furthermore, the η_α are taken to be distributed randomly across the population of neurons according to a probability density $\rho(\eta)$ which does not generate correlations between the η's at different sites, ie $\langle \eta_\alpha \eta_\beta \rangle_\eta = 0$ for $\alpha \neq \beta$. Hence, $\widetilde{Q}_{\alpha\beta} = (E +$

$\eta_\alpha)\delta_{\alpha,\beta}$ and the long time somatic response is

$$\lim_{t\to\infty} V_0(t) \equiv V^\infty(E) = S^{(e)} E \int_0^\infty \mathrm{d}t' \sum_{\beta\neq 0} a_\beta \mathrm{e}^{-Et'} \left[\exp\left(\mathbf{Q} - \mathrm{diag}(\eta)\right)t'\right]_{0\beta} \tag{56}$$

Writing $\widehat{G}_{\alpha\beta}(t) = G_{\alpha\beta}(t)\mathrm{e}^{-Et}$, and recognizing $G_{\alpha\beta}(t)$ as the Green's function of an infinite nonuniform chain where the source of nonuniformity is the random background η_α, the response (56) takes the form

$$V^\infty(E) = S^{(e)} E \sum_{\beta\neq 0} a_\beta \mathcal{G}_{0\beta}(E) \tag{57}$$

and $\mathcal{G}_{\alpha\beta}(E)$ is the Laplace transform of $G_{\alpha\beta}(t)$.

In the absence of noise we have simply that $\mathcal{G}_{\alpha\beta}(t) = \mathcal{G}^{(0)}_{\alpha\beta}(t) = [\mathrm{e}^{\mathbf{Q}^{(0)}t}]_{\alpha\beta}$(after redefining $\mathbf{Q}^{(0)} = \mathbf{Q}$) where

$$\begin{aligned} \mathcal{G}^{(0)}_{\alpha\beta}(E) &= \int_0^\infty \mathrm{d}t' \mathrm{e}^{-Et'} \left[\mathrm{e}^{\mathbf{Q}^{(0)}t}\right]_{\alpha\beta} \\ &= \int_{-\pi}^{\pi} \frac{\mathrm{d}k}{2\pi} \frac{\mathrm{e}^{ik|\alpha-\beta|}}{\epsilon(k)+E} \end{aligned} \tag{58}$$

and we have employed the integral representation (24) for the Green's function on an infinite compartmental chain. The integral (58) may be written as a contour integral on the unit circle C in the complex plane. That is, introducing the change of variables $z = \mathrm{e}^{ik}$ and substituting for $\epsilon(k)$ using (25),

$$\mathcal{G}^{(0)}_{\alpha\beta}(E) = \oint_{\mathrm{C}} \frac{\mathrm{d}z}{2\pi i} \frac{z^{|\alpha-\beta|}}{(E+\tau^{-1}+2\gamma^{-1})z - \gamma^{-1}(z^2+1)} \tag{59}$$

The denominator in the integrand has two roots

$$\lambda_\pm(E) = 1 + \frac{\gamma(E+\tau^{-1})}{2} \pm \sqrt{\left(1+\frac{\gamma(E+\tau^{-1})}{2}\right)^2 - 1} \tag{60}$$

with $\lambda_-(E)$ lying within the unit circle. Evaluating (59) we obtain

$$\mathcal{G}^{(0)}_{0\beta}(E) = \gamma \frac{(\lambda_-(E))^\beta}{\lambda_+(E) - \lambda_-(E)} \tag{61}$$

Hence, the long–time somatic response (56) with large constant excitation of the form of (51), in the absence of noise is

$$V^\infty(E) \sim S^{(e)} \sum_{\beta\neq 0} a_\beta (\lambda_-(E))^\beta \tag{62}$$

with $\lambda_-(E) \to 0$ and hence $V^\infty(E) \to 0$ as $E \to \infty$. As outlined at the end of section 3, a mean–field theory for an interacting population of such neurons

leads to a self–consistent expression for the average population firing rate in the form $E = cf(V^{\infty}(E))$ (see equation (53)). The nonlinear form of the function f introduces difficulties when one tries to perform averages over the background noise. However, progress can be made if we assume that the firing–rate is a linear function of $V^{\infty}(E)$. Then, in the presence of noise, we expect E to satisfy the self–consistency condition

$$E = c\left\langle V^{\infty}(E)\right\rangle_{\eta} + \phi \tag{63}$$

for constants c, ϕ. To take this argument to conclusion one needs to calculate the steady–state somatic response in the presence of noise and average. In fact, as we shall show, the ensemble average of the Laplace–transformed Green's function, in the presence of noise, can be obtained using techniques familiar from the theory of disordered solids[61,62]. In particular $\left\langle \mathcal{G}_{\alpha\beta}(E)\right\rangle_{\eta}$ has a general form that is a natural extension of the noise free case (58);

$$\left\langle \mathcal{G}_{\alpha\beta}(E)\right\rangle_{\eta} = \int_{-\pi}^{\pi} \frac{\mathrm{d}k}{2\pi} \frac{\mathrm{e}^{ik|\alpha-\beta|}}{\epsilon(k) + E + \Sigma(E,k)} \tag{64}$$

The so–called *self–energy* term $\Sigma(E,k)$ alters the pole structure in k–space and hence the eigenvalues $\lambda_{\pm}(E)$ in equation (60).

We note from (56) that the Laplace–transformed Green's function $\boldsymbol{\mathcal{G}}(E)$ may be written as the inverse operator

$$\boldsymbol{\mathcal{G}}(E) = [E\mathbf{I} - \mathbf{Q}]^{-1} \tag{65}$$

where $Q_{\alpha\beta} = Q^{(0)}_{\alpha\beta} - \eta_{\alpha}\delta_{\alpha,\beta}$ and $\mathbf{I}$ is the unit matrix. The following result may be deduced from (65): *The Laplace–transformed Green's function of a uniform dendritic chain with random synaptic background activity satisfies a matrix equation identical in form to that found in the tight–binding-alloy (TBA) model of excitations on a one dimensional disordered lattice*[63]. In the TBA model $\mathbf{Q}^{(0)}$ represents an effective Hamiltonian perturbed by the diagonal disorder η and E is the energy of excitation; $\left\langle \mathcal{G}_{\alpha\beta}(E)\right\rangle_{\eta}$ determines properties of the system such as the density of energy eigenstates.

Formal manipulation of (65) leads to the Dyson equation

$$\boldsymbol{\mathcal{G}} = \boldsymbol{\mathcal{G}}^{(0)} - \boldsymbol{\mathcal{G}}^{(0)}\boldsymbol{\Lambda}\boldsymbol{\mathcal{G}} \tag{66}$$

where $\boldsymbol{\Lambda} = \mathrm{diag}(\eta)$. Expanding this equation as a series in η we have

$$\mathcal{G}_{\alpha\beta} = \mathcal{G}^{(0)}_{\alpha\beta} - \sum_{\gamma} \mathcal{G}^{(0)}_{\alpha\gamma}\eta_{\gamma}\mathcal{G}^{(0)}_{\gamma\beta} + \sum_{\gamma,\gamma'} \mathcal{G}^{(0)}_{\alpha\gamma}\eta_{\gamma}\mathcal{G}^{(0)}_{\gamma\gamma'}\eta_{\gamma'}\mathcal{G}^{(0)}_{\gamma'\beta} - \ldots \tag{67}$$

Diagrams appearing in the expansion of the full Green's function equation (66) are shown in figure 6. The exact summation of this series is generally not possible.

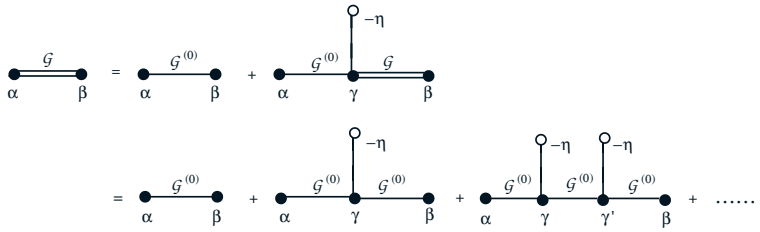

Figure 6: Diagrams appearing in the expansion of the single–neuron Green's function (67).

The simplest and crudest approximation is to replace each factor η_γ by the site–independent average $\overline{\eta}$. This leads to the so–called *virtual crystal approximation* (VCA) where the series (67) may be summed exactly to yield

$$\langle \boldsymbol{\mathcal{G}}(E) \rangle_\eta = [E\mathbf{I} - (\mathbf{Q}^{(0)} - \overline{\eta}\mathbf{I})]^{-1} = \boldsymbol{\mathcal{G}}^{(0)}(E + \overline{\eta}) \tag{68}$$

That is, statistical fluctuations associated with the random synaptic inputs are ignored so that the ensemble averaged Green's function is equivalent to the Green's function of a uniform dendritic chain with a modified membrane time constant such that $\tau^{-1} \to \tau^{-1} + \overline{\eta}$. The ensemble–average of the VCA Green's function is shown diagrammatically in figure 7. Another technique commonly applied to the

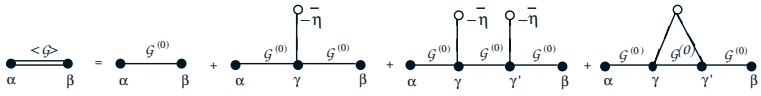

Figure 7: Diagrams appearing in the expansion of the ensemble–averaged Green's function (68).

summation of infinite series like (67) splits the sum into one over repeated and un–repeated indices. The repeated indices contribute the so–called renormalized background (see figure 8),

$$\begin{aligned} \widetilde{\eta}_\alpha &= \eta_\alpha - \eta_\alpha \mathcal{G}^{(0)}_{\alpha\alpha}\eta_\alpha + \eta_\alpha \mathcal{G}^{(0)}_{\alpha\alpha}\eta_\alpha \mathcal{G}^{(0)}_{\alpha\alpha}\eta_\alpha \ldots \\ &= \frac{\eta_\alpha}{1 + \eta_\alpha \mathcal{G}^{(0)}_{00}} \end{aligned} \tag{69}$$

where we have exploited the translational invariance of $\boldsymbol{\mathcal{G}}^{(0)}$. Then, the full series becomes

$$\mathcal{G}_{\alpha\beta} = \mathcal{G}^{(0)}_{\alpha\beta} - \sum_{\gamma \neq \alpha,\beta} \mathcal{G}^{(0)}_{\alpha\gamma}\widetilde{\eta}_\gamma \mathcal{G}^{(0)}_{\gamma\beta} + \sum_{\gamma \neq \alpha,\gamma';\gamma' \neq \beta} \mathcal{G}^{(0)}_{\alpha\gamma}\widetilde{\eta}_\gamma \mathcal{G}^{(0)}_{\gamma\gamma'}\widetilde{\eta}_{\gamma'} \mathcal{G}^{(0)}_{\gamma'\beta} - \ldots \tag{70}$$

Note that nearest neighbour site indices are excluded in (70). If an ensemble average

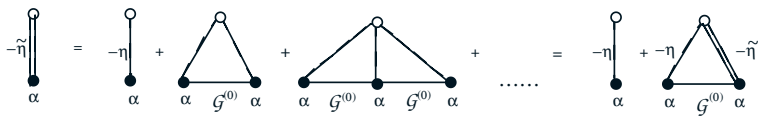

Figure 8: Diagrammatic representation of the renormalized synaptic background activity (69).

of (70) is performed, then higher–order moments contribute less than they do in the original series (67). Therefore, an improvement on the VCA approximation is expected when $\widetilde{\eta}_\alpha$ in (70) is replaced by the ensemble average $\overline{\eta}(E)$ where

$$\overline{\eta}(E) = \int \mathrm{d}\eta \rho(\eta) \frac{\eta}{1 + \eta \mathcal{G}_{00}^{(0)}(E)} \tag{71}$$

The resulting series may now be summed to yield an approximation $\widetilde{\boldsymbol{\mathcal{G}}}(E)$ to the ensemble averaged Green's function as

$$\widetilde{\boldsymbol{\mathcal{G}}}(E) = \boldsymbol{\mathcal{G}}^{(0)}(E + \widetilde{\Sigma}(E)) \tag{72}$$

where

$$\widetilde{\Sigma}(E) = \frac{\overline{\eta}(E)}{1 - \overline{\eta}(E)\mathcal{G}_{00}^{(0)}(E)} \tag{73}$$

The above approximation is known in the theory of disordered systems as the *average t–matrix approximation* (ATA).

The most effective single–site approximation used in the study of disordered lattices is the *coherent potential approximation* (CPA). In this framework each dendritic compartment has an effective (site–independent) background synaptic input $\widehat{\Sigma}(E)$ for which the associated Green's function is

$$\widehat{\boldsymbol{\mathcal{G}}}(E) = \boldsymbol{\mathcal{G}}^{(0)}(E + \widehat{\Sigma}(E)) \tag{74}$$

The self–energy term $\widehat{\Sigma}(E)$ takes into account any statistical fluctuations via a self–consistency condition. Note that $\widehat{\boldsymbol{\mathcal{G}}}(E)$ satisfies a Dyson equation

$$\widehat{\boldsymbol{\mathcal{G}}} = \boldsymbol{\mathcal{G}}^{(0)} - \boldsymbol{\mathcal{G}}^{(0)} \mathrm{diag}(\widehat{\Sigma}) \widehat{\boldsymbol{\mathcal{G}}} \tag{75}$$

Solving (75) for $\boldsymbol{\mathcal{G}}^{(0)}$ and substituting into (66) gives

$$\boldsymbol{\mathcal{G}} = \widehat{\boldsymbol{\mathcal{G}}} - \mathrm{diag}(\eta - \widehat{\Sigma}) \boldsymbol{\mathcal{G}} \tag{76}$$

To facilitate further analysis and motivated by the ATA scheme we introduce a renormalized background field $\widehat{\eta}$ as

$$\widehat{\eta}_\alpha = \frac{\eta_\alpha - \widehat{\Sigma}(E)}{1 + (\eta_\alpha - \widehat{\Sigma}(E)) \widehat{\mathcal{G}}_{00}}, \tag{77}$$

and perform a series expansion of the form (70) with $\boldsymbol{\mathcal{G}}^{(0)}$ replaced by $\widehat{\boldsymbol{\mathcal{G}}}$ and η by $\widehat{\eta}$. Since the self–energy term $\widehat{\Sigma}(E)$ incorporates any statistical fluctuations we should recover $\widehat{\boldsymbol{\mathcal{G}}}$ on performing an ensemble average of this series. Ignoring multi–site correlations, this leads to the self–consistency condition

$$\langle \widehat{\eta}_\alpha \rangle_\eta \equiv \int \mathrm{d}\eta \rho(\eta) \frac{\eta_\alpha - \widehat{\Sigma}(E)}{1 + (\eta_\alpha - \widehat{\Sigma}(E)) \mathcal{G}_{00}^{(0)}(E + \widehat{\Sigma}(E))} = 0 \tag{78}$$

This is an implicit equation for $\widehat{\Sigma}(E)$ that can be solved numerically.

The steady–state behaviour of a network can now be obtained from (57) and (63) with one of the schemes just described. The self–energy can be calculated for a given density $\rho(\eta)$ allowing the construction of an an approximate Green's function in terms of the Green's function in the absence of noise given explicitly in (61). The mean–field consistency equation for the firing–rate in the CPA scheme takes the form

$$E = cS^{(e)} E \sum_\beta a_\beta \mathcal{G}_{0\beta}^{(0)}(E + \widehat{\Sigma}(E)) + \phi \tag{79}$$

Bressloff[63] has studied the case that $\rho(\eta)$ corresponds to a Bernoulli distribution. It can be shown that the firing–rate decreases as the mean activity across the network increases and increases as the variance increases. Hence, synaptic background activity can influence the behaviour of a neural network and in particular leads to a reduction in a network's steady–state firing–rate. Moreover, a uniform background reduces the firing–rate more than a randomly distributed background in the example considered.

If the synaptic background is a time-dependent additive stochastic process, equation (55) must be replaced by

$$\overline{E}_\alpha(t) = \sum_{\beta \neq \alpha} E_\beta + \eta_\alpha(t) + \overline{E} \tag{80}$$

for some stochastic component of input $\eta_\alpha(t)$. The constant $\overline{E}$ is chosen sufficiently large to ensure that the the rate of inhibition is positive and hence physical. The presence of time–dependent shunting currents would seem to complicate any analysis since the Green's function of (54) must be replaced with

$$\mathbf{G}(t,s) = \mathbf{T}\left[\exp\left(\int_s^t \mathrm{d}t' \mathbf{Q}(t')\right)\right], \quad Q_{\alpha\beta}(t) = Q_{\alpha\beta}^{(0)} - (E + \overline{E} + \eta_\alpha(t))\delta_{\alpha,\beta} \tag{81}$$

which involves time–ordered products and is not time–translation invariant. However, this invariance is recovered when the Green's function is averaged over a *stationary* stochastic process[64]. Hence, in this case the averaged somatic membrane potential has a unique steady–state given by

$$\langle V^\infty(E) \rangle_\eta = S^{(e)} E \sum_{\beta \neq 0} a_\beta \mathcal{H}_{0\beta}(E) \tag{82}$$

where $\boldsymbol{\mathcal{H}}(E)$ is the Laplace transform of the averaged Green's function $\mathbf{H}(t)$ and

$$\mathbf{H}(t-s) = \langle \mathbf{G}(t,s) \rangle_{\eta} \tag{83}$$

The average firing–rate may be calculated in a similar fashion as above with the aid of the *dynamical* coherent potential approximation. The averaged Green's function is approximated with

$$\boldsymbol{\mathcal{H}}(E) = \boldsymbol{\mathcal{G}}^{(0)}(E + \Lambda(E) + \overline{E}) \tag{84}$$

analogous to equation (74), where $\Lambda(E)$ is determined self–consistently. Details of this approach when $\eta_{\alpha}(t)$ is a multi–component dichotomous noise process are given elsewhere[65]. The main result is that a fluctuating background leads to an increase in the steady–state firing–rate of a network compared to a constant background of the same average intensity. Such an increase grows with the variance and the correlation of the coloured noise process.

5. Neurodynamics

In previous sections we have established that the passive membrane properties of a neuron's dendritic tree can have a significant effect on the spatio–temporal processing of synaptic inputs. In spite of this fact, most mathematical studies of the dynamical behaviour of neural populations neglect the influence of the dendritic tree completely. This is particularly surprising since, even at the passive level, the diffusive spread of activity along the dendritic tree implies that a neuron's response depends on (i) previous input history (due to the existence of distributed delays as expressed by the single–neuron Green's function), and (ii) the particular locations of the stimulated synapses on the tree (i.e. the distribution of axo–dendritic connections). It is well known that delays can radically alter the dynamical behaviour of a system. Moreover, the effects of distributed delays can differ considerably from those due to discrete delays arising, for example, from finite axonal transmission times[66]. Certain models do incorporate distributed delays using so–called α functions or some more general kernel[67]. However, the fact that these are not linked directly to dendritic structure means that feature (ii) has been neglected.

In this section we examine the consequences of extended dendritic structure on the neurodynamics of nerve tissue. First we consider a recurrent analog network consisting of neurons with identical dendritic structure (modelled either as set of compartments or a one–dimensional cable). The elimination of the passive compartments (dendritic potentials) yields a system of integro–differential equations for the active compartments (somatic potentials) alone. In fact the dynamics of the dendritic structure introduces a set of continuously distributed delays into the somatic dynamics. This can lead to the destabilization of a fixed point and the simultaneous creation of a stable limit cycle via a super–critical Andronov–Hopf bifurcation.

The analysis of integro–differential equations is then extended to the case of spatial pattern formation in a neural field model. Here the neurons are continuously

distributed along the real line. The diffusion along the dendrites for certain configurations of axo–dendritic connections can not only produce stable spatial patterns via a Turing–like instability, but has a number of important dynamical effects. In particular, it can lead to the formation of time–periodic patterns of network activity in the case of *short–range inhibition* and *long–range excitation*. This is of particular interest since physiological and anatomical data tends to support the presence of such an arrangement of connections in the cortex, rather than the opposite case assumed in most models.

Finally, we consider the role of dendritic structure in networks of *integrate–and–fire* neurons[51,69,70,71,38,72,72]. In this case we replace the smooth synaptic input, considered up till now, with a more realistic train of current pulses. Recent work has shown the emergence of collective excitations in integrate–and–fire networks with local excitation and long–range inhibition[73,74], as well as for purely excitatory connections[54]. An integrate–and–fire neuron is more biologically realistic than a firing–rate model, although it is still not clear that details concerning individual spikes are important for neural information processing. An advantage of firing–rate models from a mathematical viewpoint is the differentiability of the output function; integrate–and–fire networks tend to be analytically intractable. However, the *weak*–coupling transform developed by Kuramoto and others[39,75] makes use of a particular nonlinear transform so that network dynamics can be re–formulated in a *phase*–interaction picture rather than a *pulse*–interaction one[67]. The problem (if any) of non–differentiability is removed, since interaction functions are differentiable in the phase–interaction picture, and traditional analysis can be used once again. Hence, when the neuronal output function is differentiable, it is possible to study pattern formation with *strong* interactions and when this is not the case, a phase reduction technique may be used to study pulse–coupled systems with weak interactions. We show that for long–range excitatory coupling, the phase–coupled system can undergo a bifurcation from a stationary synchronous state to a state of travelling oscillatory waves. Such a transition is induced by a correlation between the effective delays of synaptic inputs arising from diffusion along the dendrites and the relative positions of the interacting cells in the network. There is evidence for such a correlation in cortex. For example, recurrent collaterals of pyramidal cells in the olfactory cortex feed back into the basal dendrites of nearby cells and onto the apical dendrites of distant pyramidal cells[1,68].

5.1. *Dynamics of a recurrent analog network*

5.1.1. *Compartmental model*

Consider a fully connected network of identical compartmental model neurons labelled $i = 1, \ldots, N$. The system of dendritic compartments is coupled to an additional somatic compartment by a single junctional resistor r from dendritic compartment $\alpha = 0$. The membrane leakage resistance and capacitance of the soma are

denoted $\hat{R}$ and $\hat{C}$ respectively. Let $V_{i\alpha}(t)$ be the membrane potential of dendritic compartment α belonging to the i^{th} neuron of the network, and let $U_i(t)$ denote the corresponding somatic potential. The synaptic weight of the connection from neuron j to the α^{th} compartment of neuron i is written W_{ij}^{α}. The associated synaptic input is taken to be a smooth function of the output of the neuron: $W_{ij}^{\alpha} f(U_j)$, for some transfer function f, which will shall take as

$$f(U) = \tanh(\kappa U) \tag{85}$$

with gain parameter κ. The function $f(U)$ may be interpreted as the short term average firing rate of a neuron (cf equation (53)). Also, $\hat{W}_{ij} f(U_j)$ is the synaptic input located at the soma. Kirchoff's laws reduce to a set of ordinary differential equations with the form:

$$\begin{aligned} C_\alpha \frac{\mathrm{d}V_{i\alpha}}{\mathrm{d}t} &= -\frac{V_{i\alpha}}{R_\alpha} + \sum_{<\beta;\alpha>} \frac{V_{i\beta} - V_{i\alpha}}{R_{\alpha\beta}} + \frac{U_i - V_{i0}}{r}\delta_{\alpha,0} \\ &\quad + \sum_j W_{ij}^{\alpha} f(U_j) + I_{i\alpha}(t) \qquad (86) \\ \hat{C} \frac{\mathrm{d}U_i}{\mathrm{d}t} &= -\frac{U_i}{\hat{R}} + \frac{V_{i0} - U_i}{r} + \sum_j \hat{W}_{ij} f(U_j) + \hat{I}_i(t), \quad t \geq 0 \qquad (87) \end{aligned}$$

where $I_{i\alpha}(t)$ and $\hat{I}_i(t)$ are external input currents. The set of equations (86) and (87) are a generalisation of the standard graded response Hopfield model to the case of neurons with dendritic structure[31]. Unlike for the Hopfield model there is no simple Lyapunov function that can be constructed in order to guarantee stability.

The dynamics of this model may be re–cast solely in terms of the somatic variables by eliminating the dendritic potentials. Considerable simplification arises upon choosing each weight W_{ij}^{α} to have the product form

$$W_{ij}^{\alpha} = W_{ij} P_\alpha, \quad \sum_\alpha P_\alpha = 1 \tag{88}$$

so that the relative spatial distribution of the input from neuron j across the compartments of neuron i is independent of i and j. Hence, eliminating the auxiliary variables $V_{i\alpha}(t)$ from (87) with an application of the variation of parameters formula yields N coupled nonlinear Volterra integro–differential equations for the somatic potentials ($V_{i\alpha}(0) = 0$);

$$\begin{aligned} \frac{\mathrm{d}U_i}{\mathrm{d}t} &= -\hat{\epsilon} U_i + \sum_j \hat{W}_{ij} f(U_j) + F_i(t) \\ &\quad + \int_0^t \mathrm{d}t' \left\{ G(t - t') \sum_j W_{ij} f(U_j(t')) + H(t - t') U_i(t') \right\} \qquad (89) \end{aligned}$$

where $\hat{\epsilon} = (\hat{R}\hat{C})^{-1} + (r\hat{C})^{-1}$

$$H(t) = (\hat{\gamma}_0\hat{\gamma})G_{00}(t) \tag{90}$$

$$G(t) = \hat{\gamma}\sum_{\beta} P_\beta G_{0\beta}(t) \tag{91}$$

with $\hat{\gamma} = (r\hat{C})^{-1}$ and $\hat{\gamma}_0 = (rC_{\alpha_0})^{-1}$ and $G_{\alpha\beta}(t)$ is the standard compartmental response described in section 2. The effective input (after absorbing $\hat{C}$ into $\hat{I}_i(t)$) is

$$F_i(t) = \hat{I}_i(t) + \hat{\gamma}\int_0^t \mathrm{d}t' \sum_{\beta} G_{0\beta}(t-t')I_{i\beta}(t') \tag{92}$$

Note that the standard Hopfield model is recovered in the limit $\gamma, \hat{\gamma} \to \infty$, or $r \to \infty$. All information concerning the passive membrane properties and topologies of the dendrites is represented compactly in terms of the convolution kernels $H(t)$ and $G(t)$. These in turn are prescribed by the response function of each neuronal tree.

To simplify our analysis, we shall make a number of approximations that do not alter the essential behaviour of the system. First, we set to zero the effective input ($F_i(t) = 0$) and ignore the term involving the kernel $H(t)$ ($\hat{\gamma}_0\hat{\gamma}$ sufficiently small). The latter arises from the feedback current from the soma to the dendrites. We also consider the case when there is no direct stimulation of the soma, ie $\hat{W}_{ij} = 0$. Finally, we set $\kappa = 1$. Equation (89) then reduces to the simpler form

$$\frac{\mathrm{d}U_i}{\mathrm{d}t} = -\hat{\epsilon}U_i + \int_0^t G(t-t')\sum_j W_{ij} f(U_j(t'))\mathrm{d}t' \tag{93}$$

We now linearize equation (93) about the equilibrium solution $\mathbf{U}(t) = \mathbf{0}$, which corresponds to replacing $f(U)$ by U in equation (93), and then substitute into the linearized equation the solution $U_i(t) = \mathrm{e}^{zt}U_{0i}$. This leads to the characteristic equation

$$z + \hat{\epsilon} - W_i\mathcal{G}(z) = 0 \tag{94}$$

where W_i, $i = 1, \ldots, N$ is an eigenvalue of $\mathbf{W}$ and $\mathcal{G}(z) = \hat{\gamma}\sum_\beta P_\beta \mathcal{G}_{0\beta}(z)$ with $\mathcal{G}_{0\beta}(z)$ the Laplace transform of $G_{0\beta}(t)$. A fundamental result concerning integro–differential equations is that an equilibrium is stable provided that none of the roots z of the characteristic equation lie in the right–hand complex plane[76]. In the case of equation (94), this requirement may be expressed by theorem 1 of[77]: The zero solution is locally asymptotically stable if

$$|W_i| < \hat{\epsilon}/\mathcal{G}(0), \quad i = 1, \ldots, N \tag{95}$$

We shall concentrate attention on the condition for marginal stability in which a pair of complex roots $\pm i\omega$ cross the imaginary axis, a prerequisite for an Andronov–Hopf bifurcation. For a *super–critical* Andronov–Hopf bifurcation, after loss of stability of the equilibrium all orbits tend to a unique stable limit cycle that surrounds

the equilibrium point. In contrast, for a *sub–critical* Andronov–Hopf bifurcation the periodic limit cycle solution is unstable when the equilibrium is stable. Hence, the onset of stable oscillations in a compartmental model neural network can be associated with the existence of a super–critical Andronov–Hopf bifurcation.

It is useful to re–write the characteristic equation (94) for pure imaginary roots, $z = i\omega$, and a given complex eigenvalue $W = W' + iW''$ in the form

$$i\omega + \hat{\epsilon} - (W' + iW'') \int_0^\infty \mathrm{d}t \mathrm{e}^{-i\omega t} G(t) = 0, \quad \omega \in \mathbb{R} \tag{96}$$

Equating real and imaginary parts of (96) yields

$$W' = [\hat{\epsilon} C(\omega) - \omega S(\omega)]/[C(\omega)^2 + S(\omega)^2] \tag{97}$$

$$W'' = [\hat{\epsilon} S(\omega) + \omega C(\omega)]/[C(\omega)^2 + S(\omega)^2] \tag{98}$$

with $C(\omega) = \mathrm{Re}\ \mathcal{G}(i\omega)$ and $S(\omega) = -\mathrm{Im}\ \mathcal{G}(i\omega)$.

To complete the application of such a linear stability analysis requires specification of the kernel $G(t)$. A simple, but illustrative example, is a two compartment model of a soma and single dendrite, without a somatic feedback current to the dendrite and input to the dendrite only. In this case we write the electrical connectivity matrix $\mathbf{Q}$ of equation (16) in the form $Q_{00} = -{\tau_1}^{-1}$, $Q_{11} = -{\tau_2}^{-1}$, $Q_{01} = 0$ and $Q_{10} = \gamma^{-1}$ so that the somatic response function becomes:

$$\frac{\tau_1 \tau_2}{\gamma(\tau_1 - \tau_2)} \left[\mathrm{e}^{-t/\tau_1} - \mathrm{e}^{-t/\tau_2} \right] \tag{99}$$

Taking ${\tau_2}^{-1} \gg {\tau_1}^{-1}$ in (99) gives a somatic response as $\gamma^{-1}\tau_2/\mathrm{e}^{-t/\tau_1}$. This represents a kernel with *weak* delay in the sense that the maximum response occurs at the time of input stimulation. Taking $\tau_1 \to \tau_2 \to \tau$, however, yields $\gamma^{-1} t \mathrm{e}^{-t/\tau}$ for the somatic response, representing a *strong* delay kernel. The maximum response occurs at time $t + \tau$ for an input at an earlier time t. Both of these generic kernels uncover features present for more realistic compartmental geometries[77] and are worthy of further attention. The stability region in the complex W plane can be obtained by finding for each angle $\theta = \tan^{-1}(W''/W')$ the solution ω of equation (96) corresponding to the smallest value of $|W|$. Other roots of (96) produce larger values of $|W|$, which lie outside the stability region defined by ω. (The existence of such a region is ensured by theorem 1 of[77]).

Weak delay

Consider the kernel $G(t) = \tau^{-1}\mathrm{e}^{-t/\tau}$, so that $\mathcal{G}(z) = (z\tau + 1)^{-1}$, and

$$S(\omega) = \frac{\omega\tau}{1 + (\omega\tau)^2}, \quad C(\omega) = \frac{1}{1 + (\omega\tau)^2} \tag{100}$$

¿From equations (97), (98) and (100), the boundary curve of stability is given by the parabola

$$W' = \hat{\epsilon} - \frac{\tau (W'')^2}{(1 + \hat{\epsilon})^2} \tag{101}$$

and the corresponding value of the imaginary root is $\omega = W''/(1+\hat{\epsilon})$. It follows that for real eigenvalues ($W'' = 0$) there are no pure imaginary roots of the characteristic equation (96) since $\omega = 0$. Thus, for a connection matrix $\mathbf{W}$ that only has real eigenvalues, (eg a symmetric matrix), destabilization of the zero solution occurs when the largest positive eigenvalue increases beyond the value $\hat{\epsilon}/\mathcal{G}(0) = \hat{\epsilon}$, and this corresponds to a real root of the characteristic equation crossing the imaginary axis. Hence, oscillations cannot occur via an Andronov–Hopf bifurcation.

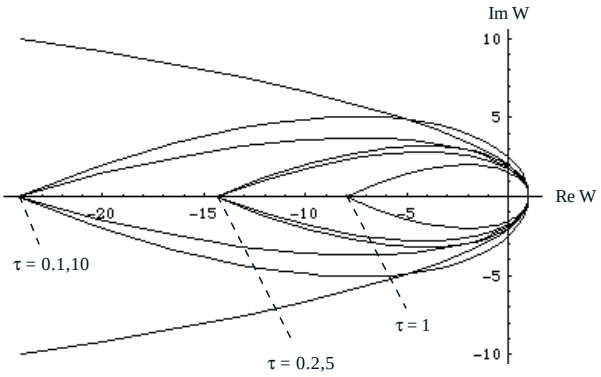

Fig. 9. Stability region (for the equilibrium) in the complex W plane for a recurrent network with generic delay kernels, where W is an eigenvalue of the interneuron connection matrix $\mathbf{W}$. For a weak delay kernel, the stability region is open with the boundary curve given by a parabola. On the other hand, the stability region is closed in the strong delay case with the boundary curve crossing the real axis in the negative half–plane at a τ–dependent value W^-. This is shown for various values of the delay τ with the decay rate $\hat{\epsilon}$ and gain κ both set to unity. All boundary curves meet on the positive half of the real axis at the same point $W^+ = \hat{\epsilon} = 1$.

Strong delay

Consider the kernel $G(t) = \tau^{-2} t \mathrm{e}^{-t/\tau}$, so that $\mathcal{G}(z) = (z\tau + 1)^{-2}$, and

$$S(\omega) = \frac{2\omega\tau}{[1 + (\omega\tau)^2]^2}, \quad C(\omega) = \frac{1 - \omega^2\tau^2}{[1 + (\omega\tau)^2]^2} \tag{102}$$

The solution of (97) and (98) is

$$W' = \hat{\epsilon}(1 - \omega^2\tau^2) - 2\omega^2\tau \tag{103}$$

$$W'' = 2\hat{\epsilon}\omega\tau + \omega(1 - \omega^2\tau^2) \tag{104}$$

Equations (103) and (104) define a parametric curve in the complex W plane, and the boundary of the stability region is shown in figure 9 for a range of delays τ. Since the stability region closes in the left half plane, it is now possible for the equilibrium to lose stability when the largest negative eigenvalue crosses the boundary, even when this eigenvalue is real. Whether or not this leads to an Andronov–Hopf bifurcation can only be determined with further analysis. For the case of real

eigenvalues the points of destabilization W^+, W^- are defined by $W'' = 0$ and equation (95). Using (95), (103) and (104) we have

$$W^+ = \hat{\epsilon}, \quad W^- = -(4\hat{\epsilon} + 2\tau^{-1} + 2\hat{\epsilon}^2\tau) \tag{105}$$

Thus, W^+ is independent of the delay τ, although W^- is not. The most appropriate way to determine if a compartmental network can support oscillations via an Andronov–Hopf bifurcation is through the transfer function approach of Allwright[78]. The conditions under which destabilization of an equilibrium is associated with the appearance or disappearance of a periodic solution are described by Bressloff[77].

5.1.2. *Semi–infinite cable*

Since the integral equation formulation of compartmental neural network dynamics (89) has a well defined continuum limit, all results can be taken over easily to the corresponding cable model. For example, suppose that the dendritic tree is represented by a semi–infinite cable $0 \leq \xi < \infty$ with the soma connected to the end $\xi = 0$. The cable equation then yields the following system of equations (cf. (86) and (87))

$$\frac{dU_i(t)}{dt} = -\frac{U_i(t)}{\hat{\tau}} + \rho_0[V_i(0,t) - U_i(t)] \tag{106}$$

$$\frac{\partial V_i(\xi,t)}{\partial t} = D\frac{\partial^2 V_i(\xi,t)}{\partial \xi^2} - \frac{V_i(\xi,t)}{\overline{\tau}} + \sum_j W_{ij}(\xi) f(U_j(t)) \tag{107}$$

Here $I_i(t) = \rho_0[V_i(0,t) - U_i(t)]$ is the current density flowing to the soma from the cable at $\xi = 0$. We have assumed for simplicity that there are no external inputs

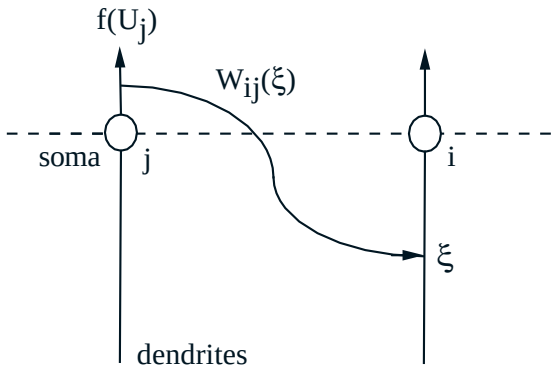

Fig. 10. Basic interaction picture for neurons with dendritic structure.

and no synaptic connections directly on the soma. Equation (107) is supplemented by the boundary condition

$$-\left.\frac{\partial V}{\partial \xi}\right|_{\xi=0} = I_i(t) \tag{108}$$

The basic interaction picture is illustrated in figure 10.

We can eliminate the dendritic potentials $V_i(\xi,t)$ since they appear linearly in equation (107). Using a standard Green's function approach[79], one obtains a solution for $V_i(0,t)$ of the form

$$\begin{aligned} V_i(0,t) &= 2\int_{-\infty}^{t} \mathrm{d}t' \int_0^{\infty} d\xi' G(\xi', t-t') \sum_j W_{ij}(\xi') f(U_j(t')) \\ &\quad -2\rho_0 \int_{-\infty}^{t} \mathrm{d}t' G(0, t-t') \left[V_i(0,t') - U_i(t')\right] \end{aligned} \tag{109}$$

where $G(\xi,t)$ is the fundamental solution of the one–dimensional cable equation (4). (The additional factor of 2 in equation (109) is due to the fact that we have a semi–infinite cable with a reflecting boundary). To simplify our analysis, we shall assume that the second term on the right–hand side of equation (109) is negligible compared to the first term arising from synaptic inputs. This approximation, which corresponds to imposing the homogeneous boundary condition $\partial V/\partial\xi|_{\xi=0} = 0$, does not alter the essential behaviour of the system. As in the analysis of the compartmental model, we assume that the distribution of axo–dendritic weights can be decomposed into the product form $W_{ij}(\xi) = P(\xi)W_{ij}$. Substituting equation (109) into (106) then leads to the integro–differential equation (93) with $\hat{\epsilon} = \hat{\tau}^{-1} + \rho_0$ and $G(t) = 2\rho_0 \int_0^{\infty} P(\xi)G(\xi,t)\mathrm{d}\xi$. For concreteness, we shall take $P(\xi) = \delta(\xi - \xi_0)$ and set $\rho_0 = 1/2$ so that $G(t) = G(\xi_0, t)$.

Linear stability analysis now proceeds along identical lines to the compartmental model with the Laplace transform $\mathcal{G}(z)$ of $G(t)$ given by

$$\mathcal{G}(z) = \frac{1}{2\sqrt{\epsilon + z}} \exp\left(-\xi_0\sqrt{\epsilon + z}\right), \quad \epsilon = \overline{\tau}^{-1} \tag{110}$$

where we have set the diffusion constant as $D = 1$. Thus we obtain equations (97) and (98) with

$$C(\omega) = \frac{1}{2\sqrt{\epsilon^2 + \omega^2}} \mathrm{e}^{-A(\omega)\xi_0} \left[A(\omega)\cos\left(B(\omega)\xi_0\right) - B(\omega)\sin\left(B(\omega)\xi_0\right)\right] \tag{111}$$

$$S(\omega) = \frac{1}{2\sqrt{\epsilon^2 + \omega^2}} \mathrm{e}^{-A(\omega)\xi_0} \left[A(\omega)\sin\left(B(\omega)\xi_0\right) + B(\omega)\cos\left(B(\omega)\xi_0\right)\right] \tag{112}$$

and $\sqrt{\epsilon + i\omega} = A(\omega) + iB(\omega)$ where

$$A(\omega) = \sqrt{[\sqrt{\epsilon^2 + \omega^2} + \epsilon]/2}, \quad B(\omega) = \sqrt{[\sqrt{\epsilon^2 + \omega^2} - \epsilon]/2} \tag{113}$$

Equations (98), (111) and (112) imply that for real eigenvalues ($W'' = 0$) the points of destabilization are

$$W^+ = \frac{\hat{\epsilon}}{C(0)} = \hat{\epsilon}\sqrt{\epsilon}\mathrm{e}^{\sqrt{\epsilon}\xi_0}, \quad W^- = \frac{\hat{\epsilon}}{C(\omega_0)}, \tag{114}$$

where ω_0 is the smallest, non–zero positive root of the equation

$$-\frac{\omega}{\hat{\epsilon}} = H(\omega, \xi_0) \equiv \left[\frac{A(\omega)\sin\left(B(\omega)\xi_0\right) + B(\omega)\cos\left(B(\omega)\xi_0\right)}{A(\omega)\cos\left(B(\omega)\xi_0\right) - B(\omega)\sin\left(B(\omega)\xi_0\right)}\right] \tag{115}$$

$H(\omega, \xi_0)$ is plotted as a function of ω in figure 11 for $\xi_0 = 2$. We are interested in the points of intersection of $H(\omega, \xi_0)$ with the straight line through the origin having slope $-\hat{\epsilon}$. We ignore the trivial solution $\omega = 0$ since this corresponds to a static instability. Although there is more than one non–zero positive solution to equation (115), we need only consider the smallest solution ω_0 since this will determine the stability or otherwise of the resting state with respect to an Andronov–Hopf bifurcation. Since the point ω_0 lies on the second branch of $H(\omega, \xi_0)$, it follows that $C(\omega_0)$ and hence W^- is negative.

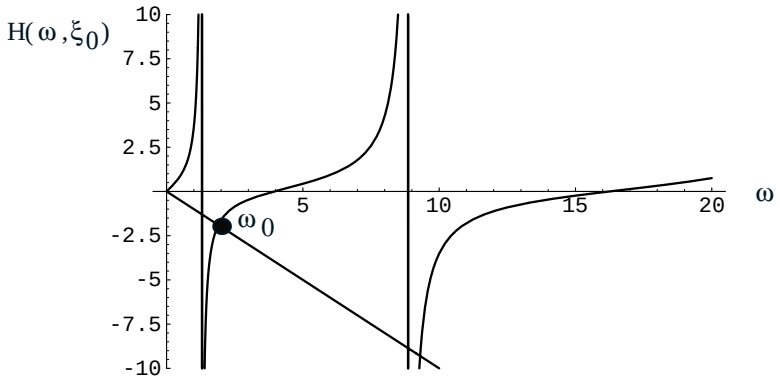

Fig. 11. Plot of function $H(\omega, \xi_0)$.

5.2. *Neural pattern formation*

We now show how the presence of spatial structure associated with the arrangement of the neurons within the network allows the possibility of *Turing* or *diffusion–driven* instability leading to the formation of spatial patterns. The standard mechanism for pattern formation in spatially organized neural networks is based on the competition between local excitatory and more long–range inhibitory lateral interactions between cells[80,33]. This has been used to model ocular dominance stripe formation in the visual cortex[81,82] and the generation of visual hallucination patterns[83]. It also forms a major component in self–organizing networks used to model the formation of topographic maps. In these networks, the lateral connections are fixed

whereas input connections to the network are modified according to some Hebbian learning scheme (see eg[36]). All standard models specify the distribution of lateral connections solely as a function of the separation between presynaptic and postsynaptic neurons, whereas details concerning the spatial location of a synapse on the dendritic tree of a neuron are ignored.

In this section we analyse a model of neural pattern formation that takes into account the combined effect of diffusion along the dendritic tree and recurrent interactions via axo–dendritic synaptic connections[84,85]. For concreteness, we consider a one–dimensional recurrent network of analog neurons. The associated integral equation, after eliminating the dendritic potentials, is obtained from equation (93) by the replacements $U_i(t) \to U(x,t)$ and $W_{ij} \to W(x,x')$. We also impose the homogeneity condition $W(x,x') = W_0 J(x-x')$ with $J(x)$ a symmetric function of x. The result is the integro–differential equation of the form

$$\frac{\partial U(x,t)}{\partial t} = -\hat{\epsilon} U(x,t) + W_0 \int_{-\infty}^{t} \mathrm{d}t' G(t-t') \int_{-\infty}^{\infty} \mathrm{d}x' J(x-x') f(U(x',t')) \quad (116)$$

Note that in the special case $G(t-t') = \delta(t-t')$, equation (116) reduces to the standard form

$$\frac{\partial U(x,t)}{\partial t} = -\hat{\epsilon} U(x,t) + W_0 \int_{-\infty}^{\infty} \mathrm{d}x' J(x-x') f(U(x',t)) \quad (117)$$

which is the basic model of nerve tissue studied previously by a number of authors[80,33].

Although pattern formation is principally a nonlinear phenomenon, a good indication of expected behaviour can be obtained using linear stability analysis. We begin by considering the reduced model described by equation (117). First, linearize about the zero homogeneous solution $U(x) \equiv 0$. Substituting into the linearized equation a solution of the form $U(x,t) = U_0 \mathrm{e}^{zt+ipx}$, where p is the wavenumber of the pattern and z is the so called growth factor, then leads to the characteristic equation

$$z + \hat{\epsilon} = W_0 \widetilde{J}(p) \quad (118)$$

where $\widetilde{J}(p)$ is the Fourier transform of $J(x)$. Denote the solution of equation (118) by $z(p)$. A Turing–like instability is said to arise if and only if

(A) Re $z(0) < 0$ (the zero solution is stable to homogeneous perturbations)

(B) there exists at least one non–zero value of p for which Re $z(p) \geq 0$.

If Re $z(p) \geq 0$ over an interval (p_1, p_2) then large–scale spatial patterns with wavenumbers in this interval are expected to grow. (Such growth is bounded by the saturating nonlinearities within the system). The stability and shape of the resulting patterns of network activity, which depend on the specific nonlinearities and the choice of initial conditions, can generally only be determined by computer simulation. Note that the pattern is stationary if Im $z(0) = 0$ at the bifurcation

point (static Turing instability), whereas a time–periodic spatial pattern can form if Im $z(0) \neq 0$ (dynamic Turing instability). For the reduced system described by equation (117), $z(p)$ is real for all p since $J(x)$ is assumed to be a symmetric function of x, and hence a dynamic Turing instability cannot occur.

Let us investigate the occurrence of static patterns. That is, we assume that z is real and look for the onset of a Turing instability as specified by conditions (A) and (B) above. As mentioned previously, the usual mechanism for inducing a Turing instability in the reduced model is based on the competition between local excitatory and more long–range inhibitory interactions between neurons[80,33]. Indeed, it is easy to show that a purely excitatory network with symmetric weights ($J(x) = J(-x)$) cannot support the formation of spatial patterns. For

$$|\widetilde{J}(p)| \leq 2\int_0^\infty \mathrm{d}x|J(x)||\cos px| \leq 2\int_0^\infty \mathrm{d}x|J(x)| \tag{119}$$

so that if $J(x) \geq 0$ for all x then $|\widetilde{J}(p)| \leq \widetilde{J}(0)$ and the result follows. A typical choice for $J(x)$ is the so–called Mexican hat function (see figure 12a). This can be constructed in terms of a difference of two exponentials, for example,

$$J(x) = \Lambda\left[\mathrm{e}^{-\gamma_1|x|} - \Gamma\mathrm{e}^{-\gamma_2|x|}\right] \tag{120}$$

under the conditions $\Gamma < 1, \gamma_1 > \gamma_2 > 0$ and $\Lambda = +1$. (The case $\Lambda = -1$, which represents short–range inhibition and long–range excitation, will be considered below in the full model). The Fourier transform $\widetilde{J}(p)$ of this function,

$$\widetilde{J}(p) = 2\Lambda\left[\frac{\gamma_1}{p^2+\gamma_1^2} - \Gamma\frac{\gamma_2}{p^2+\gamma_2^2}\right] \tag{121}$$

is shown in figure 12b. Taking W_0 as a bifurcation parameter, it is clear from figure 12b that for sufficiently small W_0 the dispersion relation satisfies $z(p) < 0$ for all p. However, as W_0 is increased a critical value W_{0c} is reached such that

$$\hat{\epsilon} = W_{0c}\widetilde{J}(p_c), \quad \widetilde{J}(p_c) = \max_p\{\widetilde{J}(p)\} \tag{122}$$

Such a critical point satisfies the conditions for a Turing instability provided that $p_c \neq 0$. From equation (121) we obtain the result

$$p_c^2 = \frac{\gamma_1^2\sqrt{\Gamma\gamma_2/\gamma_1} - \gamma_2^2}{1-\sqrt{\Gamma\gamma_2/\gamma_1}} \tag{123}$$

so that $p_c \neq 0$ when $\Gamma > (\gamma_2/\gamma_1)^3$. Note that if we had taken $\Lambda = -1$ in equation (121) then $p_c = 0$ and a Turing instability does not occur.

Now consider the full model described by equation (116). The associated characteristic equation takes the form

$$z + \hat{\epsilon} - W_0\widetilde{J}(p)\mathcal{G}(z) = 0 \tag{124}$$

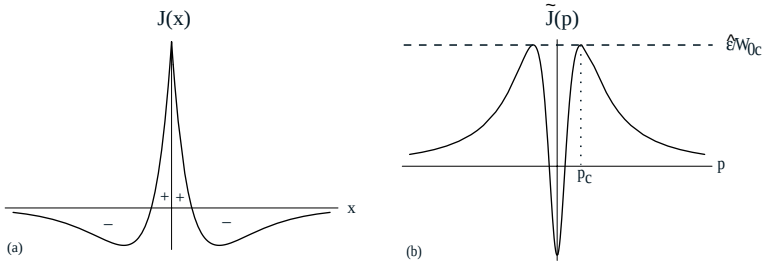

Fig. 12. Mexican hat function

In contrast to the reduced model it is now possible for dynamic instabilities to occur due to the presence of distributed delays, as realized by the kernel $\mathcal{G}(z)$. A necessary condition for dynamic pattern formation is that there exists a pair $\omega, p \neq 0$ such that

$$\hat{\epsilon} + i\omega = W_0 \widetilde{J}(p)\mathcal{G}(i\omega) \tag{125}$$

Without loss of generality, we take $\omega, p \geq 0$. Equating real and imaginary parts along identical lines to section 5.1, we obtain the following result (since $W_0\widetilde{J}(p)$ is real by assumption):

$$\hat{\epsilon} = W_0 \widetilde{J}(p)C(\omega), \quad \omega = -W_0 \widetilde{J}(p)S(\omega) \tag{126}$$

It follows that the bifurcation condition, $W_0 = W_{0c}$, for a dynamic Turing instability is

$$W_{0c}\widetilde{J}(p_{\min}) = -W^- \tag{127}$$

which should be contrasted with the bifurcation condition, $W_0 = W_{0c}^{'}$, for a static Turing instability, namely

$$W_{0c}^{'}\widetilde{J}(p_{\max}) = W^+ \tag{128}$$

where W^+, W^- are the points of destabilization as in equation (105) for strong delays and equation (114) for a semi–infinite cable, and

$$\widetilde{J}(p_{\min}) = \min_p \widetilde{J}(p), \quad \widetilde{J}(p_{\max}) = \max_p \widetilde{J}(p) \tag{129}$$

Assuming that $\widetilde{J}(p_{\min}) < 0 < \widetilde{J}(p_{\max})$, a dynamic Turing instability will occur if $W_{0c} < W_{oc}^{'}$ and $p_{\min} \neq 0$, whereas a static Turing instability will occur if $W_{0c}^{'} < W_{0c}$ and $p_{\max} \neq 0$.

In terms of the Mexican hat function (121) with $\Lambda = +1$ (short–range excitation, long–range inhibition), it is clear that a dynamic Turing instability is not possible

since $p_{\min} = 0$. However, it is possible for bulk oscillations to occur instead of static patterns when

$$\widetilde{J}(p_c) > \frac{W^+|\widetilde{J}(0)|}{W^-} \tag{130}$$

with p_c given by equation (123). On the other hand, when $\Lambda = -1$ (short–range inhibition, long–range excitation) a dynamic instability can occur since $p_{\min} = p_c$ and $p_{\max} = 0$, and provided that

$$\widetilde{J}(0) < \frac{W^+|\widetilde{J}(p_c)|}{W^-} \tag{131}$$

As recently pointed out by Swindale[36], it is surprisingly difficult to find physiological and anatomical data to support the case of short–range excitation and long–range inhibition assumed in standard models of neural pattern formation. A canonical cortical circuit appears to possess both short–range lateral inhibition and excitation together with more long–range excitatory connections[1].

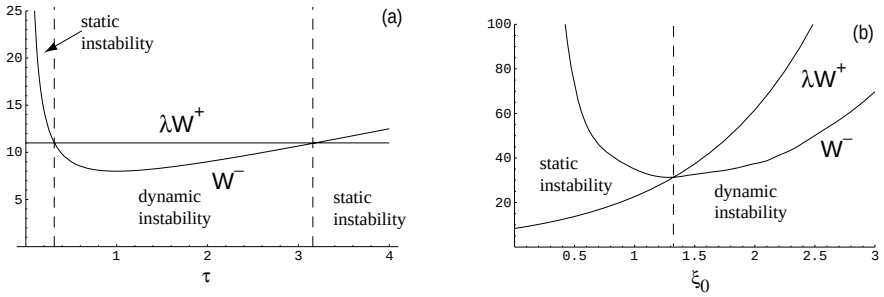

Fig. 13. Static versus dynamic instabilities: (a) two–compartment model with strong delay τ, (b) sem–infinite cable with dendritic location ξ_0.

It is interesting to consider transitions between dynamic and static instabilities as a function of the effective delay arising from dendritic structure. One finds a major difference between the strong delay kernel of a two–compartmental model and the diffusion kernel associated with a semi–infinite cable. In the former case, a dynamic instability typically occurs over a finite range of values for the effective delay τ, that is, there are two transition points, whereas in the latter case there is a single transition point as the distance ξ_0 from the soma is varied. (Note that ξ_0 determines the effective delay due to diffusion along the dendriric cable in the sense that the *time–to–peak* of the Green's function $G(\xi_0, t)$ increases with ξ_0). This difference is illustrated in figures 13a and 13b. In figure 13a we plot W^- and λW^+ as a function of τ (see equation(105)) and in figure 13b we plot W^- and λW^+ as a function of ξ_0 (see equation (114)). In both cases $\lambda = \widetilde{J}(p_{\min})/|\widetilde{J}(p_{\max})|$ is chosen

such that W^- and λW^+ intercept. In figure 14 we show a typical dynamic pattern $U(x,t)$ for $\xi_0 > \xi_{0c}$ in the case of a semi–infinite cable, where ξ_{0c} is the transition point between static and dynamic instabilities.

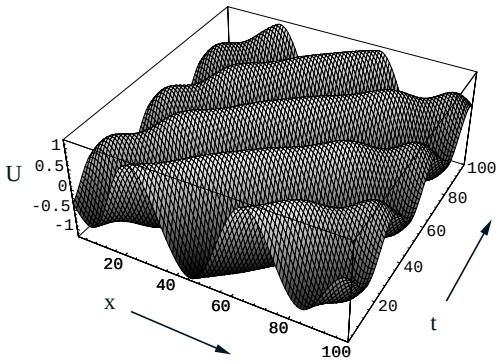

Fig. 14. Dynamic pattern formation

5.3. *Phase–synchronization in an array of integrate–and–fire neurons*

In this section we consider cell membrane properties with a nonlinear relationship between membrane ionic current and transmembrane potential[15,86] and the effect of both distributed and discrete delays on an important aspect of neurodynamics, namely synchronization of coupled neural oscillators[87,88,53,89,66]. Distributed delays are a consequence of both dendritic structure and the synaptic transmission process, whilst discrete delays arise from the finite axonal propagation velocities of action potentials. A distinction between synaptic and dendritic delay is possible since the latter only affects the response kernel of a neuron whilst the former defines synaptic input and is independent of the response kernel. We incorporate these biologically realistic features into a version of the integrate–and–fire model developed by Abbott and Kepler[90] from a systematic reduction of the Hodgkin–Huxley equations for excitable somatic tissue. The analytical intractability of this nonlinear neuronal model is much reduced with the aid of averaging techniques valid in the limit of weak coupling[39]. Indeed a nonlinear transform may be used to study interacting networks of such *pulse*–coupled neurons in a *phase*–interaction representation. In the uncoupled state a neuron is imagined to fire with a natural period T and for sufficiently weak coupling only the relative firing–phase between neurons can evolve. As we shall demonstrate, all three types of delay and the natural neuronal firing frequency in such a reduced array of *phase*–coupled oscillators can significantly affect the stability of synchronous oscillatory states and, hence, provide a mechanism for the onset of travelling waves.

5.3.1. *Synaptic and communication delays*

For concreteness, consider a one–dimensional array of nonlinear integrate–and–fire neurons distributed along the x–axis. The somatic potential $U(x,t)$ satisfies the equation

$$\frac{\partial U(x,t)}{\partial t} = f(U(x,t)) + I(x,t) \tag{132}$$

where $I(x,t)$ is the net input into the soma due to synaptic connections with other neurons in the array. When $U(x) = 1$ the neuron at x fires and is reset to $U(x) = 0$. In the absence of any synaptic input $I(x,t)$, each neuron fires with a period $T = \int_0^1 \mathrm{d}U f(U)^{-1}$. The nonlinearity f of equation (132) can be fitted to neurophysiological data using a cubic[90].

In the *weak*–coupling regime the relevant dynamical variable is the phase $\phi(x,t)$ of each oscillator, and standard phase reduction techniques may be applied[91,39,92]. In particular, following[75], we introduce the nonlinear transform

$$\phi + t/T \equiv \Psi(U) = T^{-1} \int_0^U \frac{dU'}{f(U')} \tag{133}$$

The phase variable $\phi(x,t)$ satisfies the equation

$$\frac{\partial \phi(x,t)}{\partial t} = I(x,t) F(t/T + \phi(x,t)), \quad t \in (0,T) \tag{134}$$

where $F(z) = T^{-1}/[f \circ \Psi^{-1}(z)]$, and $F(z+n) = F(z)$, $n \in \mathbb{Z}$. The neuron at x fires when $t = (n - \phi(x,t))T$ for integer n. A synaptic input spike train then takes the form

$$E(x,t) = \sum_{n=-\infty}^{0} E_s(t + [\phi(x,t) - n]T) \tag{135}$$

for $0 < t + T\phi(x,t) < T$, where $E_s(t)$ represents the post–synaptic potential. For simplicity, we shall take $E_s(t) = g\alpha^2 t \mathrm{e}^{-\alpha t}$, which is known to approximate the shape of the post–synaptic potential associated with the opening and closing of ionic channels. Note that this so–called α–function is equivalent to the strong delay kernel considered in section 5.1.1. The total synaptic input current to the soma is taken to have the form

$$I(x,t) = \frac{1}{\sigma} \int_{-\infty}^{\infty} \mathrm{d}y W(|x-y|/\sigma) E(y, t - D(|x-y|/v)) \tag{136}$$

where σ fixes the space constant of the synaptic weight kernel W and D is a delay operator dependent on the axonal propagation velocity v. For simplicity we consider $D(|x|) = |x|$.

To continue with this analysis one now assumes that t/T varies much more quickly than $\phi(x,t)$. This is valid if the system is weakly coupled. Substituting

equation (135) and (136) into equation (134) and averaging over a single period T, one finds that

$$\frac{\partial\phi(x,t)}{\partial t} = \int_{-\infty}^{\infty} \mathrm{d}y W(|y|) H(\phi(x+y,t) - \phi(x,t) - |y|/(\nu T)) \tag{137}$$

where

$$H(\phi) = \frac{1}{T}\int_0^T \mathrm{d}t \sum_{n=-\infty}^{0} E_s(t + [\phi - n]T) F(t/T) = \int_0^{\infty} \mathrm{d}\theta E_s(\theta T) F(\theta - \phi) \tag{138}$$

We have performed a change of variables so that $|x|$ now represents a dimensionless distance between the oscillators rather than position and we have introduced the parameter

$$\nu = \frac{v}{\sigma} \tag{139}$$

so that ν^{-1} has dimensions of time and characterises an effective delay. As discussed in[75], the function $F(\theta)$ is the phase interaction function of the model in the case of an instantaneous synapse. For simplicity, we shall take $F(\theta) = -\sin 2\pi\theta$, which is known to be a good approximation when f of equation (132) has an experimentally determined form[92]. In the limit $\alpha \to \infty$, $E_s(x) \to \delta(x)$, in which case $H(\phi) = \sin 2\pi\phi$ and we recover the model considered in[93].

Following Ermentrout *et al*[93], we construct travelling wave solutions of equation (137) of the form $\overline{\phi}(x,t) = \beta x + \Omega_\beta t$, with the frequency Ω_β satisfying the dispersion relation

$$\Omega_\beta = \int_{-\infty}^{\infty} \mathrm{d}y W(|y|) H(\beta y - |y|/(\nu T)) \tag{140}$$

When $\beta = 0$, the solution is synchronous. To explore the stability of the travelling wave solutions $\overline{\phi}(x,t)$, linearize equation (137) about $\overline{\phi}(x,t)$ to get

$$\frac{\partial\psi(x,t)}{\partial t} = \int_{-\infty}^{\infty} \mathrm{d}y W(|y|) H'(\beta y - |y|/(\nu T)) \left[\psi(x+y,t) - \psi(x,t)\right] \tag{141}$$

which has solutions of the form $\psi(x,t) = \mathrm{e}^{\lambda_p t + ipx}$ with

$$\lambda_p = \int_{-\infty}^{\infty} \mathrm{d}y W(|y|) H'(\beta y - |y|/(\nu T)) \left[\mathrm{e}^{ipy} - 1\right] \tag{142}$$

Note that $H'(\phi)$ indicates differentiation with respect to ϕ.

The travelling wave solution is stable provided that Re $\lambda_p < 0$ for all $p \neq 0$. (The neutrally stable mode $\lambda_0 = 0$ represents constant phase-shifts $\bar{\phi} \to \bar{\phi} + \delta$). The function $H(\phi)$ involves the convolution of the instantaneous interaction function $F(\theta)$ with the synaptic transmission function $E_s(\theta T)$ and may be written as

$$H(\phi) = A \sin 2\pi\phi - B \cos 2\pi\phi \tag{143}$$

where

$$A = [(2\pi)^2 - (\alpha T)^2]K, \quad B = -4\pi\alpha T K, \quad K = \frac{-g\alpha^2 T}{[(2\pi)^2 + (\alpha T)^2]^2} \tag{144}$$

Note the non-trivial dependence of the dynamical behaviour on the period T of the oscillators. This should be contrasted with the analysis of Ermentrout *et al*[93] who simply assume a particular form for the phase interaction function $H(\phi)$, rather than deriving it from an explicit model. In our case, $H(\phi)$ depends explicitly on both the properties of the synaptic interactions and the period of neuronal oscillation. Substituting (143) into (142) shows that

$$\text{Re } \lambda_p = \pi[\Lambda(p, 2\pi\hat{\beta}) + \Lambda(-p, 2\pi\tilde{\beta})] \tag{145}$$

where

$$\begin{aligned} \Lambda(p,\beta) &= A[W_c(p+\beta) + W_c(p-\beta) - 2W_c(\beta)] \\ &+ B[W_s(p+\beta) - W_s(p-\beta) - 2W_s(\beta)] \end{aligned} \tag{146}$$

with $\hat{\beta} = \beta - 1/(\nu T)$, $\tilde{\beta} = -\beta - 1/(\nu T)$, $W_c(p) = \int_0^\infty \mathrm{d}y W(y)\cos(py)$ and $W_s(p) = \int_0^\infty \mathrm{d}y W(y)\sin(py)$. For example, if the interaction kernel has the form $W(x) =$

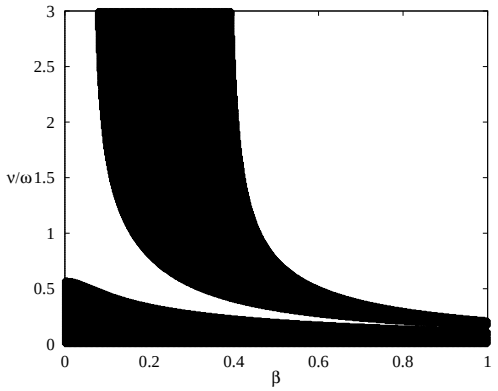

Fig. 15. $W(x) = \mathrm{e}^{-|x|}$. Stability diagram of ν/ω vs β with $\alpha/\omega = 1$. Black (white) regions denote stable (unstable) solutions.

$\mathrm{e}^{-|x|}$ then $W_c(p) = (1+p^2)^{-1}$ and $W_s(p) = p/(1+p^2)^{-1}$. In this case (and also for the case $W(x) = \Theta(1-|x|)$) the stability of travelling waves is solely determined by the propagation delay time ν^{-1}, the synaptic rise time α^{-1} and the natural frequency of the neuronal oscillator $\omega = 2\pi/T$. For fast rise times, in the sense that $\alpha/\omega \to \infty$, the synchronous state ($\beta = 0$) is unstable for small ν/ω and stable travelling waves appear. As the ratio ν/ω increases the synchronous solution stabilizes. Ermentrout *et al*[93] have suggested that this change in stability of the synchronous solution as the propagation delay grows is consistent with the

oscillatory behaviour observed in both visual cortex, showing a tendency towards synchrony and olfactory cortex, tending to produce travelling oscillatory waves; the latter has long–range connections and hence longer axonal delays. However, this may be an over–simplification since stability can alter rapidly in the presence of a finite ratio α/ω. In figure 15 we plot the stability of solutions as a function of the ratio ν/ω and wavenumber β for $\alpha/\omega = 1$. For a sufficiently large ratio of neuronal period to propagation delay time the synchronous state can lose stability in favour of travelling wave solutions.

5.3.2. *Dendritic delays*

In this section, we demonstrate the influence of dendritic structure on synchronization of coupled neural oscillators. The location of synaptic inputs on the dendritic tree can significantly affect the stability of synchronous oscillatory states and, hence, provides a mechanism for the onset of travelling waves[94]. A one–dimensional array of neurons, each filtering input through an idealised passive dendritic cable, is used to model the nonlinear behaviour induced by axo–dendritic interactions in neural populations. As in section 5.3.1, consider a one–dimensional array of pulse–coupled nonlinear integrate–and–fire neurons distributed along the x–axis, but now take each neuron's soma to be connected to a semi–infinite uniform dendritic cable as in section 5.1.2. The input $I(x,t)$ of equation (132) is the total current entering the soma from the cable. Eliminating dendritic potentials along identical lines to previous examples we find that $I(x,t)$ is of the form[84]

$$I(x,t) = \int_{-\infty}^{t} \mathrm{d}t' \int_{0}^{\infty} \mathrm{d}\xi' G(\xi', t-t') \int_{-\infty}^{\infty} \mathrm{d}x' W(\xi', |x-x'|) E(x', t') \qquad (147)$$

where $G(\xi,t)$ is the fundamental solution of the cable equation given by equation (3). Also, $W(\xi, |x-x'|)$ is the connection from a neuron at x' impinging on a synapse located at ξ on the dendritic cable of a neuron at x, and $E(x',t)$ represents the post–synaptic potential due to an input spike train from the neuron at x', equation (135). In the following analysis we fix length and time scales by setting $D = 1$ and $\overline{\tau} = 1$. (Thus ξ is measured in terms of electronic distance, which has typical values in the range 1–10 cm. Typical values for the membrane time constant $\overline{\tau}$ are 5–20 msec).

Introducing the phase variables $\phi(x,t)$ as described in section 5.3.1, dropping all signal communication delays ($v \to \infty$) and applying the phase reduction technique yields

$$\frac{\partial \phi(x,t)}{\partial t} = \int_{0}^{\infty} \mathrm{d}\xi' \int_{-\infty}^{\infty} \mathrm{d}y W(\xi', |y|) H(\xi', \phi(x+y,t) - \phi(x,t)) \qquad (148)$$

where

$$H(\xi, \phi) = \int_{0}^{\infty} \mathrm{d}\theta G(\xi, \theta T) F(\theta - \phi) \qquad (149)$$

Equation (148) gives the general phase equation for a network of *weakly* coupled oscillators with dendritic structure. The function $H(\xi,\phi)$ involves the convolution of the instantaneous interaction function $F(\theta)$ with the synaptic response function $G(\xi,t)$ which depends on the location ξ of the synapse on the dendritic cable. For simplicity we shall neglect the shape of the post–synaptic potential and take $F(\theta) = -\sin(2\pi\theta)$. Equation (149) may be evaluated using the following Fourier representation of the fundamental solution (2): $G(\xi,t) = (2\pi)^{-1}\int_{-\infty}^{\infty} \mathrm{d}k \mathrm{e}^{ik\xi-\epsilon(k)t}$ where $\epsilon(k) = k^2+1$. The result is

$$H(\xi,\phi) = \int_{-\infty}^{\infty} \frac{\mathrm{d}k}{2\pi} \mathrm{e}^{ik\xi} \left[A(k)\sin 2\pi\phi - B(k)\cos 2\pi\phi\right] \tag{150}$$

where

$$A(k) = \frac{\epsilon(k)}{\epsilon(k)^2+\omega^2}, \quad B(k) = \frac{\omega}{\epsilon(k)^2+\omega^2}, \quad \omega = \frac{2\pi}{T} \tag{151}$$

Travelling wave solutions of the form found in section 5.3.1 satisfy the dispersion relation

$$\Omega_\beta = \int_0^{\infty} \mathrm{d}\xi' \int_{-\infty}^{\infty} \mathrm{d}y W(\xi',|y|) H(\xi',\beta y) \tag{152}$$

Linearizing equation (148) gives

$$\frac{\partial\psi(x,t)}{\partial t} = \int_0^{\infty} \mathrm{d}\xi' \int_{-\infty}^{\infty} \mathrm{d}y W(\xi',|y|) H'(\xi',\beta y) \left[\psi(x+y,t) - \psi(x,t)\right] \tag{153}$$

which has solutions of the form $\psi(x,t) = \mathrm{e}^{\lambda_p t + ipx}$ with

$$\lambda_p = \int_0^{\infty} \mathrm{d}\xi' \int_{-\infty}^{\infty} \mathrm{d}y W(\xi',|y|) H'(\xi',\beta y) \left[\mathrm{e}^{ipy} - 1\right] \tag{154}$$

and $H'(\xi,\phi)$ indicates differentiation with respect to ϕ. Once again, the travelling wave solution will be stable provided that $\mathrm{Re}\lambda_p < 0$ for all $p \neq 0$.

We shall now study the stability of the synchronous state $\beta = 0$ using equations (149) and (154) for two general choices of the axo–dendritic weight distribution $W(\xi,x)$.

(I) Uncorrelated weight distribution

Suppose that the weight distribution has the product form (cf. section 5.1.2)

$$W(\xi,x) = P(\xi)W(x), \quad P(\xi) \geq 0, \quad \int_0^{\infty} P(\xi)\mathrm{d}\xi = 1 \tag{155}$$

In other words, the distribution of axon collaterals across the dendritic tree of a post–synaptic neuron is independent of the separation between the neuron and the corresponding pre–synaptic neuron. The distribution $P(\xi)$ determines the probability density of these axon collaterals. Substituting equation (155) into (148) generates the standard phase equation describing weakly coupled oscillator systems[91].

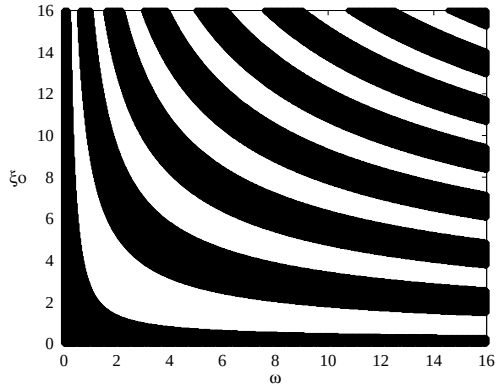

Fig. 16. Stability diagram for the uncorrelated weight distribution, ξ_0 vs ω. White (black) regions correspond to instability (stability) for the synchronous solution.

The resulting phase interaction function is given by $H(\phi) = \int_0^\infty P(\xi)H(\xi,\phi)\mathrm{d}\xi$. From equations (149), (154) and (155), the real part of the eigenvalue λ_p can be written as

$$\text{Re } \lambda_p = \frac{1}{2}\int_{-\infty}^{\infty} \mathrm{d}k\widetilde{P}(k)A(k)\left[\widetilde{W}(p+2\pi\beta)+\widetilde{W}(p-2\pi\beta)-2\widetilde{W}(2\pi\beta)\right] \qquad (156)$$

where $\widetilde{P}(k)$ and $\widetilde{W}(p)$ denote the Fourier transforms of $P(\xi)$ and $W(y)$. Suppose that the weight distribution $W(x)$ is excitatory and an exponentially decaying function of y, $W(y) = \mathrm{e}^{-\gamma|y|}/2$. The interactions are short–range (long–range) for large (small) γ. Then $\widetilde{W}(p) = \gamma/(\gamma^2+p^2)$ and one can show that the term in square brackets of equation (156) is negative (positive) when $p^2 > 12\pi^2\beta^2 - \gamma^2$ ($p^2 < 12\pi^2\beta^2 - \gamma^2$). This means that the synchronous state $\beta = 0$ will be stable (with $\gamma > 0$) if and only if $\bar{A} \equiv \int_{-\infty}^{\infty} \mathrm{d}k\widetilde{P}(k)A(k)$ is positive. To investigate the latter condition, set $P(\xi) = \delta(\xi - \xi_0)$, so that the location of each synaptic input on the dendritic tree is uniformly fixed at ξ_0. Then $\widetilde{P}(k) = \mathrm{e}^{ik\xi_0}$ and the integral $\bar{A}$ can be evaluated by closing the contour in the upper-half complex k-plane. One finds that $\bar{A}$ is positive if $\cos\left(r|\xi_0|\sin(\theta/2)+\theta/2\right) > 0$ and is negative otherwise. Here $r^2 = \sqrt{1+\omega^2}$ and $\theta = \tan^{-1}(\omega)$ with $0 \le \theta \le \pi/2$.

We deduce from the above analysis that as the distance ξ_0 of the synapse from the soma increases from zero, it reaches a critical value $\xi_{0c} = (\pi-\theta)/(2r\sin(\theta/2))$. Increasing ξ_0 further produces alternating bands of stability and instability of the synchronous state as shown in figure 16. (These regions of stability/instability would be reversed in the case of inhibitory weights). Here ξ_0, or rather the time–to–peak of the Green's function $G(\xi_0, t)$, plays an analogous role to that of an axonal time delay, since it characterizes the effective delay due to diffusion along the dendrites. We note that the time–to–peak can be as large as a few 100 msec whereas axonal delays are typically 1–10 msec (at least in myelinated fibres). It should be noted

that when the synchronous state is unstable, the solutions $\bar{\phi}(x,t)$ for all $\beta \neq 0$ are also unstable. Hence, destabilization of the synchronous state for uncorrelated weight distributions does not lead to the formation of travelling oscillatory waves. It is also clear that for this example, the range of the coupling γ^{-1} does not influence the stability of the synchronous state.

(II) Correlated weight distribution

When one considers the synaptic organization of the brain[1] one finds that the decoupling of network and dendritic co–ordinates is an over–simplification. As discussed at the start of section 5, a synapse tends to be located further away from the soma as the separation between cortical neurons increases. This results in a reduction in the effectiveness of the synaptic connection due to diffusion along the dendritic tree. Motivated by this observation concerning the synaptic organization of cortical tissue, we make the following assumption about the distribution $W(\xi,x)$: The average distance of a synapse from the soma $|\xi|$ increases with the separation $|x-x'|$ between neurons. This property can be realised by a distribution of the form

$$W(\xi,x) = W(x)\delta(|x|-\xi) \tag{157}$$

For the weight distribution (157), our model has certain formal similarities to the model considered in section 5.3.1. Long–range interactions are delayed by the effects of diffusion in the former case and by the effects of axonal transmission times in the latter case. Indeed, if one took $G(\xi,t) = \delta(t-|\xi|/\nu)$ then equations (148), (149) and (157) would formally reduce to the model of section 5.3.1 with $\alpha/\omega \to \infty$. Substituting equation (157) into equation (154) gives

$$\text{Re } \lambda_p = \frac{1}{2}\int_{-\infty}^{\infty} \mathrm{d}k A(k)[\widetilde{W}(p+k+2\pi\beta) + \widetilde{W}(p+k-2\pi\beta) - 2\widetilde{W}(k+2\pi\beta)] \tag{158}$$

In order to simplify the analysis, we shall take $W(x) = W_0\Theta(L-|x|)$ where Θ is a step function. Here L determines the range of the interactions rather than γ^{-1} as in case I. Then $\widetilde{W}(p) = 2W_0 p^{-1}\sin pL$ and

$$\text{Re } \lambda_p = \frac{1}{2}W_0\left[B(p+2\pi\beta) + B(p-2\pi\beta) - 2B(2\pi\beta)\right] \tag{159}$$

where $B(p) = 2\pi[A(p)+C(p)+C(-p)]$,

$$C(p) = \frac{\mathrm{e}^{-rL\cos\theta/2}\left[p\sin\bar{\theta} - r\cos(\bar{\theta}+\theta/2)\right]}{2r\left[p^2+r^2+2pr\sin(\theta/2)\right]} \tag{160}$$

and $\bar{\theta} = rL\sin(\theta/2) + \theta/2 + pL$ with r,θ defined as in example I.

In the limit $L \to \infty$ (all–to–all coupling), $C(p) \to 0$ and one finds from equation (159) with $B(p)$ replaced by $A(p)$ that the synchronous state is unstable if $\omega > 1$ and stable if $\omega < 1$. We also expect the synchronous state to be stable for sufficiently small values of L for all ω, since this corresponds to the limit of short–range interactions and hence small delays. We now use equations (159) and (160) to

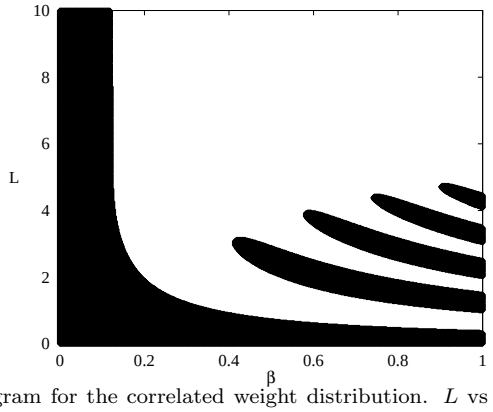

Fig. 17. Stability diagram for the correlated weight distribution. L vs β with $\omega = 1/2$. White (black) regions correspond to unstable (stable) travelling wave solutions.

determine the stability of travelling wave solutions with wavenumber β as a function of the range of coupling L. We find that if $\omega < 1$ then the synchronous state is stable for all L. On the other hand, if $\omega > 1$ then the synchronous state is unstable for large L and stable for small L. Whenever the synchronous state is unstable, there exist stable travelling wave solutions over a finite range of non-zero values of the wavenumber β. The stability region in the (β, L)–plane for $\omega = 1/2$ is shown in figure 17.

We conclude that for a correlated weight distribution, increasing the range of excitatory interactions can destabilize the synchronous state leading to the onset of stable travelling oscillatory waves when $\omega > 1$. Thus dendritic structure provides an alternative to axonal delays[93,95] as a possible mechanism underlying the differences between oscillations in the visual and olfactory cortex. The fact that bifurcations occur when $\omega = O(1)$ and $L = O(1)$ is particularly suggestive since these correspond to the typical frequencies (10–100 Hz) and length-scales (1–10 cm) relevant to cortical oscillations[96].

6. Discussion

In this review we have shown how one particular attribute of the biological neuron, namely the diffusive nature of the dendritic tree, can form the basis for a physical theory of neural tissue. Undoubtedly, many of the phenomenon seen in nerve tissue are not generated solely by diffusive processes. For example, action potentials are actively regenerated in a nonlinear fashion as they travel along the axon. Furthermore, throughout this review we have ignored some of the smaller neuronal structures, such as *spines*. Almost all excitatory inputs onto cortical pyramidal cells synapse on the tiny protrusions known as dendritic spines[97] that have been linked with the basis of memory[98]. The standard cable equation fails for such small structures and must be replaced by an electro–diffusion model that can take into account

rapid changes in ionic concentration gradients[99]. Of more concern is the fact that many spines are excitable and may nonlinearly amplify synaptic inputs[100,101] These and other complications aside, the application of *existing* physical principles allows the *rapid* development of a minimal theory of neural tissue that can be shaped by interaction with neurophysiological data.

Finally, the interplay between learning dynamics, memory retrieval, pattern formation and travelling cortical waves in a neural field possessing dendritic coordinates is a fascinating and as yet relatively unexplored area. The huge interest in artificial neural nets in the physics community relates almost exclusively to the Hopfield model and spin glass systems[7]. Many aspects of learning and memory in these systems have been thoroughly explored, and important metaphors for dynamics have been developed (basins of attraction, storage capacity etc.). Unfortunately, the direct application of results is impossible since these models have no contact with neurpophysiological data at the cellular level. By building simple, yet biologically realistic models of neural tissue, one can avoid these pitfalls, and work within a framework that has the potential to describe observed phenomenon such as cortical waves. In our analysis of neurodynamics in section 5 we concentrated on the spatio–temporal patterns associated with network output activity. However, associated with any such pattern is a corresponding pattern of activity along the dendrite of each neuron. (The latter can have a particularly non–trivial structure when there is a correlation between the location of a synapse on the dendritic tree and the positions of the interacting neurons in cortex[84,85]). A fundamental point to note within the context of learning and adaptation is that the modification of a synapse depends on both the level of pre–synaptic activity (network ouput patterns) and post–synaptic activity (dendritic patterns). Experimentally it has been found that a persistent synaptic enhancement can be induced by brief periods of synaptic activity, so–called long–term potentiation (LTP), (see eg.[102]). This typically requires the conjunction of pre–synaptic stimulation with a sufficient level of post–synaptic depolarization, which has been interpreted as a biological instance of the type of synapse underlying so–called Hebbian learning[103]. The induction of LTP appears to involve both pre– and post–synaptic mechanisms. It is thought that the post–synaptic part typically involves the influx of Ca^{2+} ions into the cell following the activation of N–methyl–D-asparate (NMDA) receptors located on a dendritic spine[104]. The pre–synaptic part is thought to involve changes in the release of neurotransmitters due to the effects of a retrograde messanger. A strong candidate for the latter is nitric oxide (NO). This is released when a post–synaptic neuron is sufficiently depolarized, and then diffuses to the pre–synaptic neuron[105]. One of the particularly interesting features of NO release is that the molecules are relatively small so that they can diffuse over quite a large neighbouring region of the post–synaptic neuron thus providing a potential mechanism for non–local learning[106]. We conclude that any analysis of learning at the network level should take into account the non–trivial relationship between patterns of output activity and patterns of dendritic activity.

Acknowledgements

The authors would like to acknowledge support from the EPSRC (UK) grant number GR/K86220.

1. G M Shepherd. Introduction to synaptic circuits. In G M Shepherd, editor, *The Synaptic Organization of the Brain*, pages 3–31. Oxford University Press, 1990.
2. B W Mel. Information processing in dendritic trees. *Neural Computation*, 6:1031–1085, 1994.
3. R Llinas and C Nicholson. Electrophysiological properties of dendrites and somata in alligator Purkinje cells. *J. Neurophysiol.*, 34:534–551, 1971.
4. Z F Mainen and T J Sejnowski. Influence of dendritic structure on firing pattern in model neocortical neurons. *Nature*, 382(25):363–366, 1996.
5. M Egelhaaf, J Haag, and A Borst. Processing of synaptic information depends on the structure of the dendritic tree. *Neuroreport*, 6(1):205–208, 1996.
6. J A Anderson and E Rosenfeld (Eds). *Neurocomputing: Foundations of Research*. MIT Press, 1988.
7. D J Amit. *Modelling Brain Function*. Cambridge University Press, 1989.
8. S Haykin. *Neural Networks: A Comprehensive Foundation*. Macmillan, 1994.
9. W Rall and I Segev. Functional possibilities for synapses on dendrites and on dendritic spines. In G M Edelman, W E Gall, and W M Cowan, editors, *Synaptic Function*. Wiley, New York, 1987.
10. J Midtgaard. Processing of information from different sources: Spatial integration in the dendrites of vertebrate CNS neurons. *Trends in Neuroscience*, 17(4):166–173, 1994.
11. G Major, A U Larkman, P Jonas, B Sakmann, and J J B Jack. Detailed passive cable models of whole–cell recorded CA3 pyramidal neurons in rat hippocampal slices. *J. Neourosci.*, 14(8):4613–4638, 1994.
12. N Spruston, D B Jaffe, and D Johnston. Dendritic attenuation of synaptic potentials and currents: The role of passive membrane properties. *Trends in Neuroscience*, 17(4):161–166, 1994.
13. H C Tuckwell. *Stochastic Processes in the Neurosciences*, volume 56 of *Ser. in Appl. Math*. SIAM, Philadelphia, 1989.
14. P S Katz and W N Frost. Intrinsic neuromodulation: Altering neuronal circuits from within. *Trends in Neuroscience*, 19(2):54–61, 1996.
15. J J B Jack, D Noble, and R W Tsien. *Electric Current Flow in Excitable Cells*. Clarendon Press, Oxford, 1975.
16. W Rall. Theory of physiological properties of dendrites. *Ann. N. Y. Acad. Sci.*, 96:1071–1092, 1962.
17. W Rall. Theoretical significance of dendritic tress for neuronal input–output relations. In R Reiss, editor, *Neural Theory and Modelling*. Stanford University Press, Stanford, 1964.
18. D H Perkel, B Mulloney, and R W Budelli. Quantitative methods for predicting neuronal behaviour. *Neuroscience*, 6(5):823–837, 1981.
19. I Segev, J W Fleshman, and R E Burke. Cable theory for dendritic neurons. In C Koch and I Segev, editors, *Compartmental Models of Complex Neurons*, pages 63–96. MIT Press, Cambridge, 1992.
20. C Itzykson and J Drouffe. *Statistical Field Theory*, volume 1 of *Cambridge Monographs on Mathematical Physics*. Cambridge University Press, Cambridge, 1989.
21. T Poggio and V Torre. A new approach to synaptic interactions. In R Heim and G Palm, editors, *Theoretical Approaches to Complex Systems*, volume 21 of *Lecture Notes in Biomathematics*, pages 89–115. Springer–Verlag, Berlin, 1978.

22. T Poggio and V Torre. A theory of synaptic interactions. In W E Reichardt and T Poggio, editors, *Theoretical Approaches in Neurobiology*, pages 28–38. MIT Press, 1981.
23. D W Dong and J J Hopfield. Dynamic properties of neural networks with adapting synapses. *Network*, 3(3):267–283, 1992.
24. J Belair, S A Campbell, and P Van Den Driessche. Frustration, stability and delay–induced oscillations in a neural network model. *SIAM J. Appl. Math.*, 56(1):245–255, 1996.
25. K Gopalsamy and I Leung. Delay induced periodicity in a neural netlet of excitation and inhibition. *Physica D*, 89:395–426, 1996.
26. A Selverston and P Mazzoni. Flexibility of computational units in invertebrate CPGs. In Mitchison and Durbin, editors, *The Computing Neuron*, chapter 11, pages 205–228. MIT Press, 1980.
27. B Mulloney and D H Perkel. The roles of synthetic models in the study of central pattern generators. In A H Cohen, S Rossignol, and S Grillner, editors, *Neural Control of Rhythmic Movements in Vertebrates*, chapter 11. Wiley, 1988.
28. A I Selverston R M Harris-Warwick, E Marder and M Moulins. *Dynamical Biological Networks: The Stomatogastric Nervous System*. MIT Press, Cambridge, 1992.
29. P L Nunez. Global contributions to cortical dynamics: Theoretical and experimental evidence for standing wave phenomena. In E Basar, editor, *Dynamics of Sensory and Cognitive Processing by the Brain*, pages 173–182. Springer–Verlag, New York, 1988.
30. G B Ermentrout and J Cowan. A mathematical theory of visual hallucination patterns. *Bio. Cybern.*, 34:137–150, 1979.
31. J J Hopfield. Neurons with graded response have collective computational properties like those of two-state neurons. *Proc. Natl. Acad. Sci.*, 81:3088–3092, 1984.
32. S Amari. Dynamics of pattern formation in lateral–inhibition type neural fields. *Bio. Cybern.*, 27:77–87, 1977.
33. U an der Heiden. Analysis of neural networks. *Lecture Notes in Mathematics*, 35:1–159, 1980.
34. H R Wilson and J D Cowan. Excitatory and inhibitory interactions in localized populations of model neurons. *Biophys. J.*, 12:1–23, 1972.
35. S Amari. Topographic organization of nerve fields. *Bull. Math. Bio.*, 42:339–364, 1980.
36. N V Swindale. The development of topography in the visual–cortex: A review of models. *Network*, 7(2):161–274, 1996.
37. K Y Tsai, N T Carnevale, and T H Brown. Hebbian learning is jointly controlled by electronic and input structure. *Network*, 5:1–19, 1994.
38. P H Chu, J G Milton, and J D Cowan. Connectivity and the dynamics of integrate–and–fire neural networks. *Int. J. Bif. Chaos*, 4(1):237–243, 1994.
39. Y Kuramoto. *Chemical Oscillations, Waves and Turbulence*. Springer-Verlag, New-York, 1984.
40. P C Bressloff and J G Taylor. Compartmental–model response function for dendritic trees. *Bio. Cybern.*, 70(2):199–207, 1993.
41. G R Grimmett and D R Stirzaker. *Probability and Random Processes*. Oxford Science Publications, Oxford, 2nd edition, 1992.
42. W Rall. Branching dendritic geometries and motoneurone membrane resistivity. *Exp. Neurol.*, 2:503–532, 1959.
43. J D Evans and G C Kember. Analytical solutions to the multicylinder somatic shunt cable model for passive neurones with differing dendritic electrical parameters. *Bio. Cybern.*, 71:547–557, 1994.
44. B G Butz and J Cowan. Transient potentials in dendritic systems of arbitrary geometry.

Biophys. J., 14:661–689, 1974.
45. L F Abbott, E Fahri, and S Gutmann. The path integral for dendritic trees. *Bio. Cybern.*, 66:49–60, 1991.
46. B J Cao and L F Abbott. A new computational method for cable theory problems. *Biophys. J.*, 64:303–313, 1993.
47. P C Bressloff, V M Dwyer, and M J Kearney. Sum–over–paths approach to diffusion on trees. *J. Phys. A*, 29:1881–1896, 1996.
48. F Rosenblatt. *Principles of Neurodynamics*. Spartan, New York, 1962.
49. P C Bressloff. Temporal processing in neural neworks with adaptive short term memory: A compartmental model approach. *Network*, 4:155–175, 1993.
50. W Rall. Time constant and electronic length of membrane cylinders and neurons. *Biophys. J.*, 9(1483):1509, 1969.
51. J P Keener, F C Hoppensteadt, and J Rinzel. Integrate–and–fire models of nerve membrane response to oscillatory input. *SIAM J. Appl. Math.*, 41(3):503–517, 1981.
52. L F Abbott and C Van Vresswijk. Asynchronous states in networks of pulse–coupled oscillators. *Phys. Rev. E*, 48(2):1483–1490, 1993.
53. W Gerstner and J L Van Hemmen. Coherence and incoherence in a globally coupled ensemble of pulse–emitting units. *Phys. Rev. Lett.*, 71(3):312–315, 1993.
54. J J Hopfield and A V M Herz. Rapid local synchronisation of action potentials: Toward computation with coupled integrate-and-fire neurons. *Proc. Natl. Acad. Sci.*, 92:6655–6662, 1995.
55. J P Rospars and P Lansky. Stochastic model neuron without resetting of dendritic potential: Application to the olfactory system. *Bio. Cybern.*, 69:283–294, 1993.
56. P C Bressloff. Dynamics of a compartmental integrate–and–fire neuron with somatic potential reset. *Physica D*, 80:399–412, 1995.
57. L F Abbott. Realistic synaptic inputs for model neural networks. *Network*, 2:245–258, 1991.
58. S Amari. Characteristics of random nets of analog neuron–like elements. *IEEE Trans. Syst. Man Cybern.*, SMC-2:643–657, 1972.
59. O Bernander, R J Douglas, K A C Martin, and C Koch. Synaptic background activity influences spatiotemporal integration in single pyramidal cells. *Proc. Natl. Acad. Sci USA*, 88:11569–11573, 1991.
60. M Rapp, Y Yarom, and I Segev. The impact of parallel fiber background activity on the cable properties of cerebellar Purkinje cells. *Neural Computation*, 4:518–533, 1992.
61. R J Elliot, J A Krumhansl, and P L Leath. The theory and properties of randomly disordered crystals and related physical systems. *Rev. Mod. Phys.*, 46:465–543, 1974.
62. J M Ziman. *Models of Disorder*. Cambridge University Press, Cambridge, 1979.
63. P C Bressloff. A Greens–function approach to analyzing the effects of random synaptic background activity in a model neural–network. *J. Phys. A*, 27(12):4097–4113, 1994.
64. R Kubo. Stochastic Liouville equation. *J. Math. Phys.*, 4(2):174–183, 1963.
65. P C Bressloff. Average firing-rate of a model neural network with dynamical disorder. *J. Phys. A*, 28:2457–2469, 1995.
66. S Coombes and G J Lord. Desynchronisation of pulse–coupled integrate–and–fire neurons. *Phys. Rev. E*, 55(3):2104R–2107R, 1997.
67. W Gerstner. Time structure of the activity in neural–network models. *Phys. Rev. E*, 51(1):738–758, 1995.
68. M A Wilson and J M Bower. Cortical oscillations and temporal interactions in a computer simulation of piriform cortex. *J. Neurophysiol*, 67:981–995, 1992.
69. H C Tuckwell. *Introduction to Theoretical Neurobiology*, volume 1. (Linear cable theory and dendritic structure) of *Cambridge Studies in Mathematical Biology*. Cambridge University Press, 1988.

70. C Van Vreeswijk and L F Abbott. Self–sustained firing in populations of integrate–and–fire neurons. *SIAM J. Appl. Maths*, 53(1):253–264, 1993.
71. M Tsodyks, I Mitkov, and H Sompolinsky. Pattern of synchrony in inhomogeneous networks of oscillators with pulse interactions. *Phys. Rev. Lett.*, 71(8):1280–1283, 1993.
72. A Corral, C J Perez, A Diaz-Guilera, and Alex Arenas. Self–organized criticality and synchronization in a lattice model of integrate–and–fire oscillators. *Phys. Rev. Lett.*, 74(1):118–121, 1995.
73. M Usher, M Stemmler, C Koch, R Ritz, J L van Hemmen, and Z Olami. Network amplification of local fluctuations causes high spike rate variability, fractal firing patterns and oscillatory local–field potentials. *Neural Computation*, 6(5):795–836, 1994.
74. M Usher and M Stemmler. Dynamic pattern formation leads to 1/f noise in neural populations. *Phys. Rev. Lett.*, 74(2):326–329, 1995.
75. C Van Vreeswijk and L F Abbott. When inhibition not excitation synchronizes neural firing. *J. Comp. Neurosci.*, 1:313–321, 1994.
76. R K Miller. Asymptotic stability properties of linear Volterra integro–differential equations. *J. Diff. Eqns.*, 10:485–506, 1971.
77. P C Bressloff. Dynamics of compartmental model recurrent neural networks. *Phys. Rev. E*, 50(3):2308–2319, 1994.
78. D J Allwright. Harmonic balance and the Hopf bifurcation. *Math. Proc. Cambridge Philos. Soc.*, 82:453–467, 1977.
79. E Zauderer. *Partial Differential Equations*. John Wiley and Sons, Singapore, 1989.
80. J D Murray. *Mathematical Biology*. Biomathematics texts. Springer, 2nd edition, 1993.
81. N V Swindale. Model for the formation of ocular dominance stripes. *Proc. Roy. Soc. Lond.*, B208:243–264, 1980.
82. E Erwin, K Obermayer, and K Schulten. Models of orientation and ocular dominance columns in the visual cortex: A critical comparison. *Neural Computation*, 7(3):425–468, 1995.
83. G B Ermentrout and J D Cowan. Large scale spatially organized activity in neural nets. *SIAM J. Appl. Maths*, 38:1–21, 1980.
84. P C Bressloff. New mechanism for neural pattern formation. *Phys. Rev. Lett.*, 76:4644–4647, 1996.
85. P C Bressloff and B D Souza. Neural pattern formation in networks with dendritic structure. preprint, 1997.
86. Daniel Johnston and Samuel Miao–Sin Wu. *Foundations of Cellular Neurophysiology*. MIT Press, Cambridge, 1995.
87. R E Mirollo and S H Strogatz. Synchronisation of pulse–coupled biological oscillators. *SIAM J. Appl. Maths*, 50(6):1645–1662, 1990.
88. Y Kuramoto. Collective synchronisation of pulse–coupled oscillators and pulse–coupled excitable units. *Physica D*, 50:15–30, 1991.
89. S Bottani. Pulse–coupled relaxation oscillators: From biological synchronization to self–organized criticality. *Phys. Rev. Lett.*, 74(21):4189–4192, 1995.
90. L F Abbott and T B Kepler. Model neurons: From Hodgkin–Huxley to Hopfield. In L Garrido, editor, *Statistical Mechanics of Neural Networks*, pages 5–18. Springer–Verlag, 1990.
91. G B Ermentrout and N Kopell. Frequency plateaus in a chain of weakly coupled oscillators. *SIAM J. Math Anal.*, 15:215–237, 1984.
92. D Hansel, G Mato, and C Meunier. Phase dynamics for weakly coupled Hodgkin–Huxley neurons. *Europhys. Lett.*, 23(5):367–372, 1993.
93. G B Ermentrout, S M Crook, and J M Bower. Connectivity, axonal delay, and synchrony

in cortical oscillators. *J. Comp. Neurosci. (To appear)*, 1996.
94. P C Bressloff and S Coombes. Synchrony in an array of integrate–and–fire neurons with dendritic structure. *Phys. Rev. Lett (Submitted)*, 1997.
95. S M Crook. *The role of delay in oscillatory models of olfactory cortex*. PhD thesis, University of Maryland, 1996.
96. C M Gray and W Singer. Stimulus–specific neuronal oscillations in orientation columns of cat visual–cortex. *Proc. Natl. Acad. Sci.*, 86:1698–1702, 1989.
97. C Koch and A Zador. The function of dendritic spines: Devices subserving biochemical rather than electrical compartmentalization. *J. Neurosci.*, 13(2):413–422, 1993.
98. A Zador, C Koch, and T H Brown. Biophysical model of a Hebbian synapse. *Proc. Natl. Acad. Sci.*, 87:6718–6722, 1990.
99. N Qian and T J Sejnowski. An electro–diffusion model for computing membrane potentials and ionic concentrations in branching dendrites, spines and axons. *Bio. Cybern.*, 62:1–15, 1989.
100. J P Miller, W Rall, and J Rinzel. Synaptic amplification by active membrane in dendritic spines. *Brain Research*, 325:325–330, 1985.
101. G M Shepherd, R K Brayton, J P Miller, I Segev, J Rinzel, and W Rall. Signal enhancement in distal cortical dendrites by means of interactions between active dendritic spines. *Proc. Natl. Acad. Sci.*, 82:2192–2195, 1985.
102. S Maren and M Baudry. Properties and mechanisms of long–term synaptic plasticity in thr mammalian brain. *Neurobiology of learning and memory*, 63:1–18,1995.
103. D O Hebb. *The Organization of Behaviour*, Wiley, New York, 1949.
104. A Zador, C Koch and T H. Brown. Biophysical model of a Hebbian synapse. *Proc. Natl. Acad. Sci*, 87: 6718-6722, 1985.
105. J Garthwatite and C Boulton. Nitric Oxide signalling in the central nervous system *Ann. Rev. Physiol.*, 57: 683–706, 1995.
106. B Krekelberg and J G Taylor. Nitric oxide: what can it compute? *Network*, 8: 1, 1997.